Title.

Expanding GABAergic Neuronal Diversity in iPSC-Derived Disease Models

Ruiqi Hu[1, 2, 3, 4, 8], Linda L. Boshans[1, 2, 3, 4, 8], Bohan Zhu[5], Peiwen Cai[5], Yiran Tao[1, 2, 3, 4], Mark Youssef[1, 2, 3, 4], Gizem Inak Girrbach[1, 2, 3, 4], Yingnan Song[5,6,7], Xuran Wang[5,6,7], Alexander Tsankov[5], Joseph D. Buxbaum[5,6,7], Sai Ma[5], Nan Yang[1,2,3,4,9]

1. Nash Family Department of Neuroscience, Friedman Brain Institute, Icahn School of Medicine at Mount Sinai, New York, NY, 10029, USA
2. Alper Center for Neurodevelopment and Regeneration, Icahn School of Medicine at Mount Sinai, New York, NY 10029, USA.
3. Institute for Regenerative Medicine, Icahn School of Medicine at Mount Sinai, New York, NY 10029, USA.
4. Black Family Stem Cell Institute, Icahn School of Medicine at Mount Sinai, New York, NY, 10029, USA
5. Department of Genetics and Genomic Sciences, Icahn School of Medicine at Mount Sinai, New York, NY 10029, USA.
6. Seaver Autism Center for Research and Treatment, Icahn School of Medicine at Mount Sinai, New York, NY 10029, USA.
7. Department of Psychiatry, Icahn School of Medicine at Mount Sinai, New York, NY 10029, USA
8. These authors contributed equally
9. Lead contact

*Correspondence: sai.ma@mssm.edu (S.M.); nan.yang1@mssm.edu (N.Y.)

Abstract

GABAergic interneurons play a critical role in maintaining neural circuit function, and their dysfunction is implicated in various neurodevelopmental and psychiatric disorders. Traditional approaches for differentiating human pluripotent stem cells (PSCs) into neuronal cells often face challenges such as incomplete neural differentiation, prolonged culture periods, and variability across PSC lines. To address these limitations, we developed a new strategy that integrates overexpression of transcription factors ASCL1 and DLX2 with dual-SMAD and WNT inhibition, efficiently driving the differentiation of human PSCs into diverse, region-specific GABAergic neuronal types. Using single-cell sequencing, we characterized the cellular heterogeneity of GABAergic induced neurons (iNs) generated with the patterning factors (patterned iNs) and those derived solely with transcription factors (PSC-derived iNs), uncovering the regulatory mechanisms that govern their fate specification. Patterned iNs exhibited gene expression features corresponding to multiple brain regions, particularly ganglionic eminence (GE) and neocortex, while GABAergic PSC-derived iNs predominantly resembled hypothalamic and thalamic neurons. Both iN types were enriched for genes relevant to neurodevelopmental and psychiatric disorders, with patterned iNs more specifically linked to neural lineage genes, highlighting their utility for disease modeling. We further applied this protocol to investigate the impact of an ADNP syndrome-associated mutation (p.Tyr719* variant) on GABAergic neuron differentiation, revealing that this mutation disrupts GABAergic fate specification and synaptic transmission. Overall, this study expands the toolkit for disease modeling by demonstrating the complementary advantages of GABAergic PSC-derived iNs and patterned iNs in representing distinct GABAergic neuron subtypes, brain regions, and disease contexts. These approaches offer a powerful platform for elucidating the molecular mechanisms underlying various neurodevelopmental and psychiatric disorders.

INTRODUCTION

Inhibitory GABAergic (GABA, γ-aminobutyric acid) neurons exhibit diverse morphology, connectivity, and physiological traits and are integral to the function of neural circuits and the modulation of complex behaviors.[1,2] Deficiencies in interneuron specification and function are linked to the pathophysiology of various neurodevelopmental and neurodegenerative disorders, including autism spectrum disorder (ASD), epilepsy, schizophrenia, and Alzheimer's disease. [3,4] Developing in vitro experimental models that can recapitulate the diverse repertoire of human interneurons holds great potential for advancing our understanding of their molecular, cellular, and physiological properties and for identifying therapeutic strategies for disorders associated with interneuron dysfunction.

Human pluripotent stem cells (PSCs) possess the remarkable ability to differentiate into a variety of cell types found throughout the body, thereby unlocking unprecedented insights into the complex biology of tissues that are typically difficult to study, especially those with unique adaptations in humans like the central nervous system (CNS). Conventional methods for neuronal differentiation sought to mimic embryonic developmental cues, employing small molecule-based patterning strategies to neuralize PSCs before steering their differentiation toward specific neuronal cell types.[5] Despite their utility, these approaches face several limitations, including partial induction of neural identities, protracted timelines required to generate mature neuronal cultures and variability in differentiation efficacies across different PSC lines.

In contrast to conventional paradigms, the direct reprogramming of PSCs into defined cell types through the forced expression of transcription factors (TFs) offers a compelling alternative. This method has been widely adopted due to its simplicity, speed, efficiency, scalability, and reproducibility. For instance, the forced expression of proneural TFs, such as Neurogenin-2 (NEUROG2 or NGN2) and achaete-scute complex-like 1 (ASCL1) - key regulators of neuronal fate during brain development - can rapidly induce neuronal differentiation in human PSCs. [6-10] However, while effective for generating neurons, this approach alone is limited in its ability to produce the full spectrum of neuronal subtypes present in the brain. Recent studies have addressed this limitation by combining TF overexpression with extrinsic patterning signals, enabling the specification of a broader range of neuronal subtypes that cannot be generated using either method alone. Notably, by promoting neuronal fate acquisition and regional patterning of human PSCs prior to forced expression of NGN2, it is possible to generate distinct populations such as cortical-like or motor neurons.[11,12] This integrated approach underscores the potential of combining genetic and chemical cues to achieve precise control over neuronal differentiation.

Despite its success in generating various neuronal subtypes, this combinatorial approach has yet to be fully explored to generate more specialized subtypes of GABAergic neurons.

Previously, we demonstrated that the forced expression of Ascl1 and Dlx2 can efficiently induce the differentiation of human PSCs into GABAergic neurons. These GABAergic induced neurons (iNs) exhibit high efficiency in adopting GABAergic neurotransmitter phenotypes and express various subtype-specific markers, indicating the generation of potentially diverse sub-populations through this protocol.[7] Despite this cellular heterogeneity, we and others have shown that GABAergic iNs are valuable for investigating inhibitory synapse-specific phenotypes linked to human neurological disorders.[7,13,14] However, the characterization of GABAergic iNs has predominantly relied on functional assays such as electrophysiology, limited analysis of a small panel of GABAergic markers by immunofluorescence, and bulk transcriptomic profiling. As a result, the precise subtype identity of these GABAergic iNs, their degree of similarity to analogous GABAergic populations in vivo, and the extent of subtype heterogeneity produced by this differentiation protocol remain largely unexplored.

To address these critical outstanding issues, we demonstrate in this study that neuralization of stem cells via dual SMAD inhibition and WNT signaling inhibition,[15] followed by forced expression of ASCL1 and DLX2, effectively specifies diverse GABAergic neuron identities that correspond to populations found in the developing forebrain. Using single-cell RNA sequencing (scRNA-seq), we comprehensively characterized GABAergic iNs generated from small molecule-patterned PSCs (patterned-iNs) and compared them with PSC-derived ASCL1/DLX2-iNs (PSC-iNs), revealing that each method produces a variety of GABAergic neuronal subtypes with a composite of brain regional identities. In addition, we explored the differentiation dynamics and regulatory mechanisms driving the fate specification of PSC-iNs and patterned-iNs through single-cell multiomics. To further demonstrate the utility of the patterned-iNs, we investigated the effects of the ADNP syndrome-associated p.Tyr719* mutation on GABAergic neuron development and function using this model system. Our results indicate that the p.Tyr719* variant disrupts the specification of certain GABAergic neuronal subtypes and impairs synaptic function in GABAergic iN cells. Overall, our study enhances the toolkit for disease modeling by demonstrating the complementary strengths of iPSC-iNs and patterned-iNs in capturing distinct GABAergic neuron subtypes, brain regions, and disease contexts. This dual approach provides a versatile platform for dissecting the molecular mechanisms underlying various neurodevelopmental and neuropsychiatric disorders.

RESULTS

ASCL1 & DLX2 Induce GABAergic Neurons from Patterned Progenitors.

Direct programming leverages one or more TFs to force the establishment of a distinct transcriptional network, thereby promoting the adoption of a new cellular identity [16,17]. Previously, we reported that forced expression of ASCL1 and DLX2 in human PSCs induces rapid differentiation into GABAergic neurons (Figure 1A). While these iN cells displayed core features of GABAergic neurons, such as GAD1/2, DLXs, and SLC32A1 (vGAT), the homogeneity of the resulting cell population or their similarity to *in vivo* counterparts remained unclear. To address these questions, we performed single-cell RNA sequencing (scRNA-seq) to profile GABAergic PSC-iNs 42 days after ASCL1 and DLX2 expression (Figure 1A).

For comparison, we generated interneurons using a well-established directed differentiation protocol that involves dual SMAD inhibition, WNT signaling inhibition, and activation of SHH signaling to specify ventral telencephalic progenitors, which give rise to interneurons.[18,19] This approach is presumed to produce GABAergic neurons similar to PSC-iNs, as evidenced by the expression of interneuron subtype markers such as Somatostatin (SST), Calretinin (CR), and Calbidin (CB). [7,18] We characterized these neurons five weeks after culturing the progenitors on dissociated mouse glial cells (Figure S1A). While neurons generated using the directed differentiation method expressed GABAergic markers like *GAD1* and *DLX6-AS*, they showed minimal expression of markers associated with synaptic function, including *SLC32A1* and *SYN1*. In contrast to PSC-iNs, these neurons expressed *FOXG1*, a defining marker of forebrain identity, suggesting that they represent immature cortical interneurons (Figures S1B and S1C). The lack of FOXG1 expression in PSC-iNs indicates that they may resemble GABAergic neurons from more posterior brain regions.

These observations prompted us to investigate whether extrinsic small molecules could synergize with ASCL1 and DLX2 to rapidly generate diverse inhibitory neurons associated with specific brain regions. To explore this, we employed a doxycycline (DOX)--responsive piggyBac transposon system for robust overexpression of ASCL1 and DLX2 in human cells. We first induced central nervous system neuroectoderm from human PSCs by inhibiting TGF-β and BMP signaling using SB431542 and LDN193189 and blocking WNT signaling with the tankyrase inhibitor XAV939. [20] After this patterning phase, DOX was applied to induce ASCL1 and DLX2 expression in these neural progenitor cells, alongside DAPT, a γ-secretase inhibitor, to eliminate dividing progenitors and synchronize maturation.[21] The cells were then dissociated and co-cultured with mouse astrocytes to promote neuronal maturation and synapse formation. In

addition, we examine if varying the duration of ASCL1 and DLX2 expression affects neuronal fate by discontinuing DOX after 3 or 7 days post-induction (3D-patterned-iNs and 7D-patterned-iNs, respectively). Five weeks after co-culturing with astrocytes, we detected GABAergic neurons expressing MAP2 and DLX2 under all experimental conditions (Figure 1A).

To gain deeper insights into these neurons, we performed scRNA-seq on neuronal cultures from each condition, analyzed alongside the GABAergic PSC-iNs. In total, we generated transcriptomes from 12,876 cells across various differentiation strategies, including 5,314 PSC-iNs, 2,899 3D-patterned-iNs, and 4,663 7D-patterned-iNs that passed quality control (Table S1). We categorized the main cell types by performing dimensionality reduction and visualized the cell clusters using uniform manifold approximation and projection (UMAP). This analysis identified seven molecularly distinct clusters of cells stratified by the differentiation approaches (Figure S2A). Further examination of neuronal marker gene expression revealed that most cells exhibit neuronal characteristics marked by *MAP2, STMN1,* and *SYN1* expression (Figures S2B and S2C). Most of the induced neurons (86.2%) are GABAergic, as indicated by the expression of *GAD1*, *GAD2*, *SLC32A1*, and *DLXs*. A small subset was identified as glutamatergic, based on *SLC17A6/7* expression (3D-patterned-iNs (42/2,899), 7D-patterned-iNs (56/4,663), PSC-iNs (10/5,314)). Only a few neurons exclusively expressed other subtype markers, such as CHAT (cholinergic, 0.02%) and TH (dopaminergic, 0.06%). We noticed that compared to 7D-patterned-iNs, a smaller proportion of cells in the 3D-patterned-iN cluster expressed the GABAergic marker *SLC32A1* (19.4% v.s. 50.9%). Conversely, a larger number of 3D-patterned-iNs exhibited genes associated with a primitive phenotype, such as *SOX2* (7.0% v.s. 0.94% in 7D-patterned-iNs). These data suggest that three days of ASCL1 and DLX2 expression is not sufficient to fully drive NPC-like cells into a mature neuronal state. Together, our data demonstrate the potential of leveraging TFs, small molecular interventions, and their synergistic effects to generate GABAergic neurons from human PSCs.

Molecularly Diverse GABAergic Neurons Generated Through Different Methods.

To further investigate the heterogeneity among the induced GABAergic neurons (iGABAs), we extracted the *SCL32A1*-expressing neurons, which included 4,086 PSC-iGABAs, 574 3D-patterned-iGABAs, and 1,915 7D-patterned-iGABAs. These neurons were categorized into five major clusters based on their gene expression patterns, with distinct separations between clusters depending on the differentiation method used (Figure 1B). As expected, all clusters consistently expressed characteristic markers of the GABAergic lineage while generally devoid of markers indicative of other neuronal types (Figures 1C and S3A). Consistent with our findings from

immunofluorescent staining [7], these clusters exhibited variable enrichment for inhibitory neuron subtype markers, such as *SST*, *CALB1*, *CALB2*, *VIP,* and *NPY* (Figures 1C and S3A). When examining the differentially expressed TFs across these clusters, we found *FOXG1* expressed in patterned-iGABAs (clusters 3 and 4). The gene expression signature of 7D-patterned-iGABAs (cluster 2) reflected spatial origins and subtypes associated with the caudal and lateral ganglionic eminences (GE), marked by *NR2F2* (*COUP-TFII*), *PAX6*, and *ISL1*. [22,23] *ISL1* was also strongly expressed in cluster 0, which consisted of PSC-iGABAs, whereas PSC-iGABAs in cluster 1 robustly expressed *FOXA2* and *NKX2-2*, markers typically associated with inhibitory neurons in the hypothalamus. [24,25] In addition to TFs, we identified differentially expressed genes (DEGs) related to ion channel proteins, neurotransmitter receptors, and calcium-binding proteins across the molecularly distinct clusters, further underscoring the molecular diversity of GABAergic neurons generated by different methods (Figure 1C and Table S2). Interestingly, the expression levels of NMDAR subunits *GRIN2A* and *GRIN2B* were notably higher in neurons produced with the small molecules (Figure S3B). *GRIN2B* expression was observed in the human cerebral cortex during prenatal stages, with some expression continuing postnatally. *GRIN2A* expression, conversely, was almost exclusively postnatal.[26] This aligns with previous findings that patterning, in conjunction with neuron lineage-specific TF induction, can enhance the expression of NMDAR subunits,[12] suggesting a synergistic effect promoting mature neuronal characteristics.

Next, to annotate the brain regional identities represented by the induced GABAergic neurons, we used a reference-mapping approach to transfer labels from existing scRNA-seq datasets of various primary human fetal brain areas [27,28], including the neocortex, GE, striatum, thalamus, hypothalamus, midbrain, and claustrum (see Methods). The GABAergic neurons are primarily mapped to a range of forebrain regions, such as the hypothalamus, thalamus, neocortex, and GE (Figure 1D). While neurons derived from all three differentiation methods exhibited characteristics of multiple brain regions, those associated with the GE and neocortex were predominantly generated using ASCL1 and DLX2 following patterning (7D-patterned-iGABAs) (Figure 1D). In contrast, neurons generated in the absence of small molecule patterning factors (PSC-iGABAs) aligned more with the hypothalamic and thalamic regions. This mapping is supported by the detection of specific markers for these brain regions, such as the expression of *FOXA2* in the hypothalamus cluster [24,29] and *NR2F2* in the GE cluster (Figure S3C).

Neuropsychiatric and Neurological Disease Gene Enrichment Across GABAergic iN Types.

Induced neurons offer significant potential for studying neuropsychiatric and neurological diseases *in vitro*, offering valuable insights for basic research and pharmaceutical development.

To assess the disease modeling capabilities of different GABAergic iN types, we conducted gene set enrichment analysis using Disease Enrichment (DisGeNET)[30] on shared and condition-specific genes from PSC- or patterned-GABAergic iNs. Our analysis revealed that genes shared between PSC- and patterned-GABAergic iNs were strongly enriched for risk genes associated with various brain disorders, including intellectual disability, neurodevelopmental disorders (NDDs), schizophrenia, epilepsy, and bipolar disorder (Figure S4, Table S3, q-value ≤ 0.05). Notably, while genes specific to patterned iNs also showed strong enrichment in psychiatric and neurological conditions, genes specific to PSC-iNs were enriched in non-neural related diseases. These findings suggest that while both PSC- and patterned iNs provide GABAergic neurons suitable for investigating disease-associated genotype-phenotype relationships, patterned iNs are more closely aligned with neural lineages, making them particularly advantageous for modeling neural-related diseases.

Gene Regulatory Networks Underlying Diverse GABAergic-Induced Neurons.

Next, we explored the regulatory mechanisms governing the cellular identities of the GABAergic neurons using single-cell regulatory network inference and clustering (SCENIC), a computational tool for deciphering regulons (i.e., groups of genes regulated by the same TF or set of TFs) to construct a detailed gene regulatory network.[31] This approach revealed distinct sets of regulons associated with different methodologies for generating GABAergic neurons, identifying unique and shared regulons across these approaches (Figure 1E). For instance, regulons associated with PSC-iGABAs included well-recognized determinants of interneuron cell fate and migration, such as DLX2 and DLX5. Regulons linked to 7D-patterned-iGABAs, such as NR2F1 (COUP-TFI), NR2F2 (COUP-TFII), and PAX6, are recognized for their roles in the differentiation of specific interneuron subtypes, including those originating from the LGE and CGE [22,32,33].

Given the limited number of GABAergic neurons obtained under the 3-day DOX exposure condition, we focused on a more detailed examination of GABAergic PSC-iNs and 7D-patterned iNs (referred to as patterned-iNs hereafter) to identify specifically activated regulons within each molecular cluster. Neurons from these conditions were categorized into distinct clusters according to their gene expression profiles, and regulons were assigned to them. We ranked regulons based on their Regulon Specificity Score (RSS) and focused on the highest-ranked ones for in-depth analysis (Figures 2A and 2B). Our analysis revealed that each neuronal cluster was associated with different sets of regulons. Specifically, within the GABAergic PSC-iNs, we identified networks regulated by TFs instrumental in regionalization, neurogenesis, and functional aspects of the hypothalamus, including FOXA1/2 and PBX1 (Figure 2A). FOXA1 and FOXA2 emerged as

primary regulons in cluster 1, aligning with prior research showing their expression in the embryonic hypothalamus and its pivotal role in adaptive behavior during fasting.[24,29] PBX1 has been implicated in hypothalamic molecular pathways affecting hormonal regulation.[34] We also showed the expression patterns of these top-ranked regulators in corresponding neuronal clusters (Figure 2A). Moreover, consistent with our findings that certain neurons resemble striatal cells, several highly expressed TFs are strongly linked to both striatal and hypothalamic differentiation and function, including ONECUTs, MEIS2, and ISL1.[23,35,36]

In contrast, we found that subclusters of GABAergic neurons generated with patterning factors were enriched in a distinct set of regulons associated with the processes of neural fate determination and migration, including *NR2F1/2, DLX6*, *RARB*, *POU2F2*, *TCF12,* and *PAX6* (Figures 2B). Notably, NR2F1, NR2F2, and PAX6 are expressed in GE and play pivotal roles in the development of cortical interneurons and inhibitory neurons in the ventromedial forebrain. Unlike the GABAergic PSC-iNs, the GABAergic patterned-iN subclusters were less distinctive, as evidenced by the more uniform expression of key regulators and the shared regulons across these groups (Figure 2C). Our analysis revealed heterogeneity among induced GABAergic neurons, with distinct gene expression profiles influenced by the differentiation methods and the specific gene regulatory networks that orchestrate the maintenance of these diverse cellular identities.

Distinct Lineage-Specific Gene Regulatory Networks Induced by ASCL1&DLX2 in PSCs and Patterned Progenitors.

Epigenetic regulation plays a pivotal role in determining and specifying cell lineages. To gain insights into the regulatory mechanisms driving the fate specification of PSC-iNs and patterned-iNs, we conducted SHARE-seq (Simultaneous High-throughput ATAC and RNA Expression with Sequencing) [37] on PSCs, patterned progenitors and cells at the early stages of differentiation induced by ASCL1 and DLX2 (Figure 3A). This approach allowed us to capture gene expression and chromatin accessibility profiles within the same cells simultaneously, offering a comprehensive view of the regulatory landscape. We successfully obtained high-quality ATAC-seq and RNA-seq data from 23,434 cells. To unravel the global similarities and distinctions among individual cells, we performed dimension reduction using Latent Semantic Indexing (LSI) on single-cell ATAC-seq data and PCA on single-cell RNA-seq data, followed by visualization using UMAP embedding. The structure of RNA and chromatin representations were well aligned, displaying the progression of cell states throughout the time course, organized by the cell type of origin (Figure 3B).

To investigate the mechanisms governing the specification of GABAergic neurons derived from PSCs and patterned progenitors, we first defined the trajectory of neuron development by assigning pseudotime values to each cell and tracing their progression along their respective differentiation pathways (Figure 4C). Not surprisingly, we observed the expression of neural progenitor cell (NPC) marker genes (e.g., *SOX2*, *NES*, *SOX11*, *PAX6*) in the patterned progenitors (Figure S5). Additionally, genes associated with interneuron development, such as *OTX2*, *PROX1*, *TCF12*, and *RELN*, were robustly induced by TF induction in the patterned progenitors and, to a lesser extent, in iPSCs (Figures 3C and S5). This expression pattern quickly transitioned to markers indicative of GABAergic neuron lineage (e.g., *GAD1*, *GAD2*, *DLX6*, etc.). The induction of neuronal genes (e.g., *DCX TUBB3, RBFOX3*, etc.) and genes encoding neurotransmitter receptors (*GRIA1-4*, *GRINA*, *GRIN2A*, *GABRA2/B2*, etc.) was detected in these differentiating cells, consistent with the rapid gene expression changes characteristic of TF-mediated cell fate conversion. Genes active late in pseudotime exhibited gene ontology (GO) enrichments related to neural morphogenesis, migration, and development (Figure 3C). Interestingly, distinctive GO enrichments were associated with genes active at early and intermediate stages of differentiation trajectories over pseudotime, suggesting that ASCL1 and DLX2 induce unique molecular changes in PSCs and patterned progenitors, respectively. For instance, GO terms exclusively enriched for genes active in early PSC-iN trajectory included non-neuronal terms. In contrast, genes induced in patterned iNs were associated with signaling pathways involved in neurogenesis, such as the WNT and VEGF signaling pathways [38-40].

Further analysis of the chromatin landscapes before and after TF induction revealed significant changes, with distinct clusters of open chromatin peaks emerging across different cell states and stages of differentiation (Figure 3D). GO analysis of genes linked to these open chromatin regions showed that regions accessible in PSCs and patterned NPC-like cells that became largely inaccessible after ASCL1 and DLX2 induction were primarily associated with non-neuronal processes (clusters 4, 5). Conversely, regions initially inaccessible in PSCs or patterned cells but became accessible post-induction were strongly associated with neurogenesis (cluster 2). We also noted that transiently accessible regions were linked to stem cell differentiation (clusters 1, 8), while regions that became robustly accessible only in the PSC-iN trajectory sometimes exhibited “off-target” effects (clusters 3, 7). Similar to the gene expression changes in response to the TFs, these findings indicate a stringent neuronal differentiation program driven by ASCL1 and DLX2 in patterned NPC-like cells, compared to a more varied gene expression program in PSCs at early stages, which underscores the nuanced interplay of epigenetic and transcriptional regulation in guiding cell fate decisions.

We subsequently examined the TF-driven regulatory mechanisms across pseudotime. By correlating TF expression with motif activity scores derived from chromatin accessibility, we identified key motifs involved in the differentiation processes. This analysis highlighted 37 TF motifs differentially associated with the progression of PSC-iNs or patterned-iNs (Figure 4E). Both differentiation pathways exhibited active ASCL1 and DLX motif activities, reinforcing their pivotal roles in cell fate determination. Additionally, motifs of TFs with known roles in neural development and function, such as TCF12, CTCF, SP3, SP9, and KLF7,[41-47] were active in both differentiation trajectories. However, numerous other TF motifs, particularly those integral for maintaining the self-renewal of pluripotent stem cells and guiding their differentiation into various lineages, including POU4F1 (OCT4), MGA, SNAI2, TCF3, and MEIS3 motifs,[48-51] were more specifically involved in the PSC-iN differentiation pathway. These findings underscore the intricate coordination of TF motifs early in neuronal differentiation, supporting our observation that ASCL1 and DLX2 drive a more tightly regulated TF network in patterned progenitors, fostering a more defined path toward neuronal differentiation. In contrast, PSCs demonstrate greater plasticity and can activate a broader spectrum of TF-driven gene expression networks, which correlates with their inherent flexibility in cell fate determination. This distinction suggests that while both PSCs and patterned progenitors are capable of neuronal differentiation, the pathways and regulatory networks involved are significantly divergent, reflecting the inherent differences in their biological potential and responsiveness to transcriptional regulators.

Disease modeling potential of patterned induced GABAergic neurons.

We next investigated whether GABAergic patterned iNs could be utilized to uncover disease phenotypes, focusing on ADNP syndrome - a rare neurodevelopmental disorder caused by mutations in the *ADNP* gene. Many individuals with ADNP syndrome exhibit symptoms consistent with ASD.[52-54] Among these patients, a recurrent heterozygous nonsense mutation at p.Tyr719* has been frequently identified.[52-54] To model this mutation, we employed CRISPR-Cas9 to introduce the *ADNP* $^{p.Tyr719*}$ mutation into two control human iPSC lines (PGP1 and WTC11). In addition, we inserted a hemagglutinin (HA) tag at the 3' end of the endogenous *ADNP* gene or immediately after p.Tyr719, allowing us to detect the full-length and truncated proteins. As shown in Figure S6, an ADNP antibody, which recognizes a region between residues 1,050 and the C-terminus of human ADNP, detected both unedited and HA-tagged full-length ADNP but not the truncated p.Tyr719* protein. The presence of the truncated p.Tyr719* protein was confirmed using the HA antibody. As expected, we observed reduced levels of the full-length protein in the heterozygous p.Tyr719* lines compared to the corresponding unedited cells.

To investigate the potential phenotypic effects of the pathogenic *ADNP* variant p.Tyr719* in GABAergic neurons, we generated patterned iNs from heterozygous and homozygous *ADNP*$^{p.Tyr719*}$ iPSCs and their isogenic control lines. Neurons were analyzed five weeks after being co-cultured with glia using scRNA-seq. Following quality control and filtering, the WTC11 homozygous line was excluded from the analysis due to an insufficient number of cells.

We first confirmed that patterned iNs were highly reproducible across different lines (Figure S6A). Transcriptomic analysis revealed a high degree of correlation between heterozygous and homozygous mutant cells (Figures 4A and 4B), leading us to combine the heterozygous and homozygous cells from both the PGP1 and WTC11 lines to increase the statistical power of our analyses. Pan-neuronal markers, such as *MAP2* and *RBFOX3* (NeuN) (Figure S6B), were robustly expressed in both wild-type and mutant cells, indicating successful neuronal differentiation. We then assessed the neurotransmitter specificity of the neurons and found that most neurons were GABAergic, with 98.62% of wild-type and 97.28% of mutant MAP2-positive neurons classified as GABAergic cells.

To further explore cellular heterogeneity, we applied the Leiden algorithm to identify clusters of transcriptomically related cells in a reduced-dimensional space. This analysis revealed a clear segregation between mutant and wild-type cells, supported by statistically significant transcriptional differences (Table S4). Specifically, clusters 0 and 1 were predominantly composed of p.Tyr719* mutant cells, whereas cluster 2 was enriched with wild-type cells (Figure 4C). We then assessed the maturation states of the affected neurons by assigning pseudotime values to each cell using Monocle3,[55,56] which revealed that mutant cells in cluster 0 represent the least mature population (Figure 4D). This finding is supported by the significant enrichment of *NESTIN* (*NES)*, a marker commonly expressed in neural progenitors, within this cluster (Table S4). The data also demonstrated a clear differentiation trajectory within the mutant cells. This pseudotemporal order of cell state transition was further validated using Slingshot (Figure S7C). As cells progressed from cluster 0 to cluster 1, there was a notable upregulation of GABA and glutamate receptor subunits (*GABRB2*, *GRIA2*, *GRID2*), synaptic signaling components (*SYN3*, *DLG2*, *NRXN3*), and neuron differentiation markers (*ROBO1*, *NRP2*), all of which are critical for neuronal growth and synaptic transmission (Figure S7D and Table S5).

To further characterize the molecular properties of the mutant GABAergic cells, we examined DEGs between mature (see Method) mutant and wild-type cells. The mutant neurons exhibited both downregulated and upregulated genes (Figure 4E). Notably, several genes involved in the generation of CGE-derived cortical interneurons, including *NR2F2* and *PROX1*, as well as LGE-

derived interneurons in the olfactory bulb and basal nuclei, such as *PAX6*, *FOXP2*, *TSHZ1,* and *CALB1*,[22] were significantly downregulated in the mutant cells. Conversely, genes like *ISL1*, associated with striatal spiny projection neurons, and *RELN*, primarily produced by a subset of GABAergic interneurons in the neocortex and hippocampus, were upregulated in the mutant cells.[57,58] Additionally, several neurotransmitter receptors and synaptic structural genes were upregulated in the mutant cells (Figure 4E). GO analysis further highlighted that the differentially expressed genes are closely associated with neuron differentiation and synaptic transmission (Figure 4F and Table S6).

To investigate the specific pathways dysregulated in *p.Tyr719** mutant neurons, we also performed Weighted Gene Co-expression Network Analysis (WGCNA) focusing on clusters 0, 1, and 2. To address the sparsity inherent in single-cell data while preserving the heterogeneity often masked by traditional cell clustering, we first constructed metacells[59] - aggregates of cells with similar gene expression profiles, where within metacells variation is primarily due to technical rather than biological sources (Figure S8A). Subsequently, we constructed gene co-expression modules separately for the three clusters, identifying 25 gene co-expression modules (Figure S8B). GO analysis revealed that the biological processes enriched in modules associated with *Tyr719** mutant include translational initiation, neuron development, membrane potential, and regulation of chemical synaptic transmission (Figure S8C). Together, our findings using GABAergic patterned-iNs suggest that the pathogenic p.Tyr719* variant not only alters the composition and characteristics of neuronal subtypes within the GABAergic lineage but also disrupts synaptic transmission in differentiated cells, which aligns with impaired neuronal excitability and synaptic transmission observed in mice with Adnp haploinsufficiency.[60]

DISCUSSION

Differentiating patient-specific stem cells into regional- and neurotransmitter-specific subtypes of human interneuron populations offers a promising platform for studying pathophysiology and potential therapeutic approaches for various diseases. This study presents a rapid and reproducible differentiation method to generate GABAergic neurons by integrating our TF-mediated PSC differentiation[7] with developmental patterning through the inhibition of SMAD and WNT signaling[15,18]. This method, akin to the direct conversion of PSCs to GABAergic neurons driven by ASCL1 and DLX2, results in a homogeneous population of cells with an inhibitory identity. We also provide an extensive minable dataset comprising single-cell RNA-seq results of GABAergic neurons generated with and without patterning molecules. This dataset uncovers unique features of neurons derived from different differentiation schemes and aids in determining the suitability of PSC-derived GABAergic neurons for studying specific genes/disorders. Additionally, the study demonstrates that this combinatorial approach produces multiple disease-relevant GABAergic neuron types and applies it to investigate the pathobiology of ADNP syndrome.

SMAD and WNT inhibitors can induce forebrain lineages from human PSCs, including excitatory and inhibitory neurons[15,18]. By activating SHH signaling, progenitor cells can be ventralized to differentiate towards human cortical interneuron lineages[18,19]. However, the maturation of these progenitor cells requires a protracted time, as evidenced by single-cell RNA-seq data. When ASCL1 and DLX2 were induced in hPSCs exposed to SMAD and WNT inhibitors, homogenous GABAergic neurons could be derived without the need for SHH or its agonist. The neurons derived under this condition represent multiple brain regions and are biased toward the cortical lineage. In contrast, PSC-iNs without patterning molecules exhibit a more prominent hypothalamic identity. Furthermore, the iPSC-iNs are enriched for TF regulons associated with hypothalamic and striatal neurogenesis and function. On the other hand, patterned iNs are enriched for TF regulons linked to neural fate determination and migration. This difference highlights the distinct developmental trajectories and functional specializations of the two types of iNs. Notably, recent work utilizing barcoding tools for lineage tracing suggested that individual human cortical progenitors can produce both excitatory and inhibitory neurons.[61] Cortically-derived inhibitory neurons share transcriptional similarities with CGE-derived interneurons but lack definitive marker genes. Given the expression of *SP8* and *NR2F2* in the patterned iNs, it is possible that some of these neurons represent cortically-derived inhibitory neurons.

The differential gene expression programs observed in PSC-derived iNs and patterned iNs generated through ASCL1 and DLX2 overexpression highlight the complexity of transcriptional regulation in neurogenesis. Multiple factors may contribute to these differences. One of the primary reasons is the differences between the epigenetic landscapes of PSCs and neural progenitor cells (NPCs) obtained via SMAD and WNT inhibition. PSCs possess a more open and plastic chromatin structure, allowing a broader range of TF binding sites to be accessible. In contrast, NPCs have a more restricted chromatin landscape, with specific regions pre-configured for neural differentiation. ASCL1, as a pioneering factor, can bind to closed chromatin regions and initiate chromatin remodeling. However, the function of pioneering factors is heavily influenced by cellular context. In PSCs, ASCL1 can access and activate a wide array of genes, leading to diverse gene expression profiles that may even include non-neuronal lineages. Conversely, the chromatin landscape in the NPCs is already more accessible in regions relevant to neural development, so ASCL1 and DLX2 primarily enhance the existing neural gene expression program. PSCs and neural progenitor cells also differ in their baseline transcriptional states. PSCs express genes associated with pluripotency and self-renewal, whereas NPCs are committed to a neural lineage and express genes related to neural progenitor characteristics. When ASCL1 and DLX2 are introduced into these different contexts, the downstream targets they activate are influenced by the pre-existing transcriptional milieu. ASCL1 and DLX2 might interact with pluripotency factors and other non-neural transcriptional networks, leading to a more heterogeneous response in PSCs. Meanwhile, these TFs reinforce and enhance the neural differentiation program in the NPCs, resulting in a more focused and streamlined gene expression profile. This aligns with the observation that GABAergic patterned-iN subtypes are less molecularly distinguishable. Additionally, the availability of co-factors and interaction partners in PSCs and neural progenitor-like cells can further modulate the activity of ASCL1 and DLX2, contributing to the observed differences in gene expression programs.

Finally, we utilized patterned GABAergic iNs to investigate the phenotypic changes caused by the ADNP syndrome-associated p.Tyr719* variant. ADNP is ubiquitously expressed and involved in chromatin remodeling and gene expression. It interacts with several proteins, including the chromodomain helicase DNA binding protein 4 (CHD4), a key component of the nucleosome remodeling and deacetylase (NuRD) complex.[62,63] Together with CHD4 and HP1γ, ADNP forms the ChAHP complex, which inhibits gene transcription.[62] In *Adnp* knockout embryonic stem (ES) cells and mouse embryos, defects in neuronal fate specification have been observed.[62] Additionally, impaired excitatory and inhibitory synapses have been reported in juvenile *Adnp* haploinsufficient mice.[60] Consistent with these findings, our data suggest that the p.Tyr719*

variant not only alters the specification of neuronal subtypes within the GABAergic lineage but may also disrupt synaptic transmission in differentiated cells. Interestingly, little difference in gene expression was observed in wild-type and heterozygous conditional *Adnp* knockout animals.[64] However, our transcriptomic analysis revealed a high degree of correlation between heterozygous and homozygous p.Tyr719* mutant GABAergic neurons. One possible explanation is that, unlike the removal of exon 5, which encodes all but 67 of Adnp's 1108 total amino acids, the p.Tyr719* variant creates a truncated protein that may exert a dominant function, competing with the full-length protein for interacting partners and DNA-binding sites.[62] Intriguingly, we observed upregulated *CHD4* expression in mutant cells, a phenomenon not seen in *Adnp* knockout cells (Figure S7B). Given that p.Tyr719* interacts with CHD4, the upregulation of CHD4 may compensate for the sequestration of CHD4 by p.Tyr719*. Future studies are needed to elucidate the precise mechanisms underlying these effects.

Overall, our study expands the toolbox for disease modeling by demonstrating the complementary strengths of iPSC-iNs and patterned iNs in representing different brain regions and disease contexts. This dual approach offers a robust platform for investigating the molecular mechanisms underlying a variety of neurodevelopmental and neuropsychiatric disorders.

Acknowledgments

This work was supported by NIH awards 5R21MH119580 (N.Y.) and 5R01NS116057 (N.Y.). This study was supported in part by the Seaver Foundation; R.H. is a Seaver Postdoctoral Fellow. L.L.B. was supported by the Training Program in Stem Cell Biology fellowship from the New York State Department of Health (NYSTEM-C32561GG). M.Y. is supported by a diversity supplement (3R01MH129372-03S1).

Author contributions

Conceptualization, R.H., L.L.B., S.M., and N.Y.; Methodology, R.H., L.L.B., B.Z., S.M., and N.Y.; Investigation, R.H., B.Z., Y. T., G.I.G., and N.Y.; Formal Analysis, L.L.B., P. C., Y.S., X. W., A.T., J.D.B., and S.M.; Writing, R.H., L.L.B., X.W., S.M., and N.Y.; Supervision, N.Y.

Declaration of interests

The authors declare no competing interests.

REFERENCES

1. Le Magueresse, C., and Monyer, H. (2013). GABAergic interneurons shape the functional maturation of the cortex. Neuron *77*, 388-405. 10.1016/j.neuron.2013.01.011.
2. Wamsley, B., and Fishell, G. (2017). Genetic and activity-dependent mechanisms underlying interneuron diversity. Nat Rev Neurosci *18*, 299-309. 10.1038/nrn.2017.30.
3. Marin, O. (2012). Interneuron dysfunction in psychiatric disorders. Nat Rev Neurosci *13*, 107-120. 10.1038/nrn3155.
4. Verret, L., Mann, E.O., Hang, G.B., Barth, A.M., Cobos, I., Ho, K., Devidze, N., Masliah, E., Kreitzer, A.C., Mody, I., et al. (2012). Inhibitory interneuron deficit links altered network activity and cognitive dysfunction in Alzheimer model. Cell *149*, 708-721. 10.1016/j.cell.2012.02.046.
5. Chambers, S.M., Fasano, C.A., Papapetrou, E.P., Tomishima, M., Sadelain, M., and Studer, L. (2009). Highly efficient neural conversion of human ES and iPS cells by dual inhibition of SMAD signaling. Nat Biotechnol *27*, 275-280. 10.1038/nbt.1529.
6. Hester, M.E., Murtha, M.J., Song, S., Rao, M., Miranda, C.J., Meyer, K., Tian, J., Boulting, G., Schaffer, D.V., Zhu, M.X., et al. (2011). Rapid and efficient generation of functional motor neurons from human pluripotent stem cells using gene delivered transcription factor codes. Mol Ther *19*, 1905-1912. 10.1038/mt.2011.135.
7. Yang, N., Chanda, S., Marro, S., Ng, Y.H., Janas, J.A., Haag, D., Ang, C.E., Tang, Y., Flores, Q., Mall, M., et al. (2017). Generation of pure GABAergic neurons by transcription factor programming. Nat Methods *14*, 621-628. 10.1038/nmeth.4291.
8. Zhang, Y., Pak, C., Han, Y., Ahlenius, H., Zhang, Z., Chanda, S., Marro, S., Patzke, C., Acuna, C., Covy, J., et al. (2013). Rapid single-step induction of functional neurons from human pluripotent stem cells. Neuron *78*, 785-798. 10.1016/j.neuron.2013.05.029.
9. Pang, Z.P., Yang, N., Vierbuchen, T., Ostermeier, A., Fuentes, D.R., Yang, T.Q., Citri, A., Sebastiano, V., Marro, S., Sudhof, T.C., and Wernig, M. (2011). Induction of human neuronal cells by defined transcription factors. Nature *476*, 220-223. 10.1038/nature10202.
10. Chanda, S., Ang, C.E., Davila, J., Pak, C., Mall, M., Lee, Q.Y., Ahlenius, H., Jung, S.W., Sudhof, T.C., and Wernig, M. (2014). Generation of induced neuronal cells by the single reprogramming factor ASCL1. Stem Cell Reports *3*, 282-296. 10.1016/j.stemcr.2014.05.020.
11. Limone, F., Guerra San Juan, I., Mitchell, J.M., Smith, J.L.M., Raghunathan, K., Meyer, D., Ghosh, S.D., Couto, A., Klim, J.R., Joseph, B.J., et al. (2023). Efficient generation of lower induced motor neurons by coupling Ngn2 expression with developmental cues. Cell Rep *42*, 111896. 10.1016/j.celrep.2022.111896.
12. Nehme, R., Zuccaro, E., Ghosh, S.D., Li, C., Sherwood, J.L., Pietilainen, O., Barrett, L.E., Limone, F., Worringer, K.A., Kommineni, S., et al. (2018). Combining NGN2 Programming with Developmental Patterning Generates Human Excitatory Neurons with NMDAR-Mediated Synaptic Transmission. Cell Rep *23*, 2509-2523. 10.1016/j.celrep.2018.04.066.
13. Sanchez-Priego, C., Hu, R., Boshans, L.L., Lalli, M., Janas, J.A., Williams, S.E., Dong, Z., and Yang, N. (2022). Mapping cis-regulatory elements in human neurons links psychiatric disease heritability and activity-regulated transcriptional programs. Cell Rep *39*, 110877. 10.1016/j.celrep.2022.110877.
14. Marro, S.G., Chanda, S., Yang, N., Janas, J.A., Valperga, G., Trotter, J., Zhou, B., Merrill, S., Yousif, I., Shelby, H., et al. (2019). Neuroligin-4 Regulates Excitatory Synaptic Transmission in Human Neurons. Neuron *103*, 617-626 e616. 10.1016/j.neuron.2019.05.043.

15. Chambers, S.M., Qi, Y., Mica, Y., Lee, G., Zhang, X.J., Niu, L., Bilsland, J., Cao, L., Stevens, E., Whiting, P., et al. (2012). Combined small-molecule inhibition accelerates developmental timing and converts human pluripotent stem cells into nociceptors. Nat Biotechnol *30*, 715-720. 10.1038/nbt.2249.
16. Graf, T., and Enver, T. (2009). Forcing cells to change lineages. Nature *462*, 587-594. 10.1038/nature08533.
17. Wang, H., Yang, Y., Liu, J., and Qian, L. (2021). Direct cell reprogramming: approaches, mechanisms and progress. Nat Rev Mol Cell Biol *22*, 410-424. 10.1038/s41580-021-00335-z.
18. Maroof, A.M., Keros, S., Tyson, J.A., Ying, S.W., Ganat, Y.M., Merkle, F.T., Liu, B., Goulburn, A., Stanley, E.G., Elefanty, A.G., et al. (2013). Directed differentiation and functional maturation of cortical interneurons from human embryonic stem cells. Cell Stem Cell *12*, 559-572. 10.1016/j.stem.2013.04.008.
19. Nicholas, C.R., Chen, J., Tang, Y., Southwell, D.G., Chalmers, N., Vogt, D., Arnold, C.M., Chen, Y.J., Stanley, E.G., Elefanty, A.G., et al. (2013). Functional maturation of hPSC-derived forebrain interneurons requires an extended timeline and mimics human neural development. Cell Stem Cell *12*, 573-586. 10.1016/j.stem.2013.04.005.
20. Ciceri, G., Baggiolini, A., Cho, H.S., Kshirsagar, M., Benito-Kwiecinski, S., Walsh, R.M., Aromolaran, K.A., Gonzalez-Hernandez, A.J., Munguba, H., Koo, S.Y., et al. (2024). An epigenetic barrier sets the timing of human neuronal maturation. Nature *626*, 881-890. 10.1038/s41586-023-06984-8.
21. Lin, Y., Yang, J., Shen, Z., Ma, J., Simons, B.D., and Shi, S.H. (2021). Behavior and lineage progression of neural progenitors in the mammalian cortex. Curr Opin Neurobiol *66*, 144-157. 10.1016/j.conb.2020.10.017.
22. Schmitz, M.T., Sandoval, K., Chen, C.P., Mostajo-Radji, M.A., Seeley, W.W., Nowakowski, T.J., Ye, C.J., Paredes, M.F., and Pollen, A.A. (2022). The development and evolution of inhibitory neurons in primate cerebrum. Nature *603*, 871-877. 10.1038/s41586-022-04510-w.
23. Shi, Y., Wang, M., Mi, D., Lu, T., Wang, B., Dong, H., Zhong, S., Chen, Y., Sun, L., Zhou, X., et al. (2021). Mouse and human share conserved transcriptional programs for interneuron development. Science *374*, eabj6641. 10.1126/science.abj6641.
24. Kim, D.W., Place, E., Chinnaiya, K., Manning, E., Sun, C., Dai, W., Groves, I., Ohyama, K., Burbridge, S., Placzek, M., and Blackshaw, S. (2022). Single-cell analysis of early chick hypothalamic development reveals that hypothalamic cells are induced from prethalamic-like progenitors. Cell Rep *38*, 110251. 10.1016/j.celrep.2021.110251.
25. Kim, D.W., Liu, K., Wang, Z.Q., Zhang, Y.S., Bathini, A., Brown, M.P., Lin, S.H., Washington, P.W., Sun, C., Lindtner, S., et al. (2021). Gene regulatory networks controlling differentiation, survival, and diversification of hypothalamic Lhx6-expressing GABAergic neurons. Commun Biol *4*, 95. 10.1038/s42003-020-01616-7.
26. Traynelis, S.F., Wollmuth, L.P., McBain, C.J., Menniti, F.S., Vance, K.M., Ogden, K.K., Hansen, K.B., Yuan, H., Myers, S.J., and Dingledine, R. (2010). Glutamate receptor ion channels: structure, regulation, and function. Pharmacol Rev *62*, 405-496. 10.1124/pr.109.002451.
27. Bhaduri, A., Sandoval-Espinosa, C., Otero-Garcia, M., Oh, I., Yin, R., Eze, U.C., Nowakowski, T.J., and Kriegstein, A.R. (2021). An atlas of cortical arealization identifies dynamic molecular signatures. Nature *598*, 200-204. 10.1038/s41586-021-03910-8.
28. Herb, B.R., Glover, H.J., Bhaduri, A., Colantuoni, C., Bale, T.L., Siletti, K., Hodge, R., Lein, E., Kriegstein, A.R., Doege, C.A., and Ament, S.A. (2023). Single-cell genomics reveals region-specific developmental trajectories underlying neuronal diversity in the human hypothalamus. Sci Adv *9*, eadf6251. 10.1126/sciadv.adf6251.

29. Silva, J.P., von Meyenn, F., Howell, J., Thorens, B., Wolfrum, C., and Stoffel, M. (2009). Regulation of adaptive behaviour during fasting by hypothalamic Foxa2. Nature *462*, 646-650. 10.1038/nature08589.
30. Pinero, J., Ramirez-Anguita, J.M., Sauch-Pitarch, J., Ronzano, F., Centeno, E., Sanz, F., and Furlong, L.I. (2020). The DisGeNET knowledge platform for disease genomics: 2019 update. Nucleic Acids Res *48*, D845-D855. 10.1093/nar/gkz1021.
31. Aibar, S., Gonzalez-Blas, C.B., Moerman, T., Huynh-Thu, V.A., Imrichova, H., Hulselmans, G., Rambow, F., Marine, J.C., Geurts, P., Aerts, J., et al. (2017). SCENIC: single-cell regulatory network inference and clustering. Nat Methods *14*, 1083-1086. 10.1038/nmeth.4463.
32. Hu, J.S., Vogt, D., Lindtner, S., Sandberg, M., Silberberg, S.N., and Rubenstein, J.L.R. (2017). Coup-TF1 and Coup-TF2 control subtype and laminar identity of MGE-derived neocortical interneurons. Development *144*, 2837-2851. 10.1242/dev.150664.
33. Zhou, X., Liu, F., Tian, M., Xu, Z., Liang, Q., Wang, C., Li, J., Liu, Z., Tang, K., He, M., and Yang, Z. (2015). Transcription factors COUP-TFI and COUP-TFII are required for the production of granule cells in the mouse olfactory bulb. Development *142*, 1593-1605. 10.1242/dev.115279.
34. Rodriguez-Zas, S.L., Southey, N.L., Rund, L., Antonson, A.M., Nowak, R.A., and Johnson, R.W. (2023). Prenatal and postnatal challenges affect the hypothalamic molecular pathways that regulate hormonal levels. PLoS One *18*, e0292952. 10.1371/journal.pone.0292952.
35. Fragkouli, A., van Wijk, N.V., Lopes, R., Kessaris, N., and Pachnis, V. (2009). LIM homeodomain transcription factor-dependent specification of bipotential MGE progenitors into cholinergic and GABAergic striatal interneurons. Development *136*, 3841-3851. 10.1242/dev.038083.
36. Su, Z., Wang, Z., Lindtner, S., Yang, L., Shang, Z., Tian, Y., Guo, R., You, Y., Zhou, W., Rubenstein, J.L., et al. (2022). Dlx1/2-dependent expression of Meis2 promotes neuronal fate determination in the mammalian striatum. Development *149*. 10.1242/dev.200035.
37. Ma, S., Zhang, B., LaFave, L.M., Earl, A.S., Chiang, Z., Hu, Y., Ding, J., Brack, A., Kartha, V.K., Tay, T., et al. (2020). Chromatin Potential Identified by Shared Single-Cell Profiling of RNA and Chromatin. Cell *183*, 1103-1116 e1120. 10.1016/j.cell.2020.09.056.
38. Barber, M., Andrews, W.D., Memi, F., Gardener, P., Ciantar, D., Tata, M., Ruhrberg, C., and Parnavelas, J.G. (2018). Vascular-Derived Vegfa Promotes Cortical Interneuron Migration and Proximity to the Vasculature in the Developing Forebrain. Cereb Cortex *28*, 2577-2593. 10.1093/cercor/bhy082.
39. Harrison-Uy, S.J., and Pleasure, S.J. (2012). Wnt signaling and forebrain development. Cold Spring Harb Perspect Biol *4*, a008094. 10.1101/cshperspect.a008094.
40. Okabe, K., Fukada, H., Tai-Nagara, I., Ando, T., Honda, T., Nakajima, K., Takeda, N., Fong, G.H., Ema, M., and Kubota, Y. (2020). Neuron-derived VEGF contributes to cortical and hippocampal development independently of VEGFR1/2-mediated neurotrophism. Dev Biol *459*, 65-71. 10.1016/j.ydbio.2019.11.016.
41. Elbert, A., Vogt, D., Watson, A., Levy, M., Jiang, Y., Brule, E., Rowland, M.E., Rubenstein, J., and Berube, N.G. (2019). CTCF Governs the Identity and Migration of MGE-Derived Cortical Interneurons. J Neurosci *39*, 177-192. 10.1523/JNEUROSCI.3496-17.2018.
42. Laub, F., Aldabe, R., Friedrich, V., Jr., Ohnishi, S., Yoshida, T., and Ramirez, F. (2001). Developmental expression of mouse Kruppel-like transcription factor KLF7 suggests a potential role in neurogenesis. Dev Biol *233*, 305-318. 10.1006/dbio.2001.0243.

43. Liu, Z., Zhang, Z., Lindtner, S., Li, Z., Xu, Z., Wei, S., Liang, Q., Wen, Y., Tao, G., You, Y., et al. (2019). Sp9 Regulates Medial Ganglionic Eminence-Derived Cortical Interneuron Development. Cereb Cortex *29*, 2653-2667. 10.1093/cercor/bhy133.
44. Moore, D.L., Blackmore, M.G., Hu, Y., Kaestner, K.H., Bixby, J.L., Lemmon, V.P., and Goldberg, J.L. (2009). KLF family members regulate intrinsic axon regeneration ability. Science *326*, 298-301. 10.1126/science.1175737.
45. Singh, A., Mahesh, A., Noack, F., Cardoso de Toledo, B., Calegari, F., and Tiwari, V.K. (2022). Tcf12 and NeuroD1 cooperatively drive neuronal migration during cortical development. Development *149*. 10.1242/dev.200250.
46. Watson, L.A., Wang, X., Elbert, A., Kernohan, K.D., Galjart, N., and Berube, N.G. (2014). Dual effect of CTCF loss on neuroprogenitor differentiation and survival. J Neurosci *34*, 2860-2870. 10.1523/JNEUROSCI.3769-13.2014.
47. Yamakawa, H., Cheng, J., Penney, J., Gao, F., Rueda, R., Wang, J., Yamakawa, S., Kritskiy, O., Gjoneska, E., and Tsai, L.H. (2017). The Transcription Factor Sp3 Cooperates with HDAC2 to Regulate Synaptic Function and Plasticity in Neurons. Cell Rep *20*, 1319-1334. 10.1016/j.celrep.2017.07.044.
48. Howard, J.M., Nuguid, J.M., Ngole, D., and Nguyen, H. (2014). Tcf3 expression marks both stem and progenitor cells in multiple epithelia. Development *141*, 3143-3152. 10.1242/dev.106989.
49. Qin, J., Wang, C., Zhu, Y., Su, T., Dong, L., Huang, Y., and Hao, K. (2021). Mga safeguards embryonic stem cells from acquiring extraembryonic endoderm fates. Sci Adv *7*. 10.1126/sciadv.abe5689.
50. Schulte, D., and Geerts, D. (2019). MEIS transcription factors in development and disease. Development *146*. 10.1242/dev.174706.
51. Zhou, W., Gross, K.M., and Kuperwasser, C. (2019). Molecular regulation of Snai2 in development and disease. J Cell Sci *132*. 10.1242/jcs.235127.
52. Van Dijck, A., Vulto-van Silfhout, A.T., Cappuyns, E., van der Werf, I.M., Mancini, G.M., Tzschach, A., Bernier, R., Gozes, I., Eichler, E.E., Romano, C., et al. (2019). Clinical Presentation of a Complex Neurodevelopmental Disorder Caused by Mutations in ADNP. Biol Psychiat *85*, 287-297. 10.1016/j.biopsych.2018.02.1173.
53. Helsmoortel, C., Vulto-van Silfhout, A.T., Coe, B.P., Vandeweyer, G., Rooms, L., van den Ende, J., Schuurs-Hoeijmakers, J.H., Marcelis, C.L., Willemsen, M.H., Vissers, L.E., et al. (2014). A SWI/SNF-related autism syndrome caused by de novo mutations in ADNP. Nat Genet *46*, 380-384. 10.1038/ng.2899.
54. Breen, M.S., Garg, P., Tang, L., Mendonca, D., Levy, T., Barbosa, M., Arnett, A.B., Kurtz-Nelson, E., Agolini, E., Battaglia, A., et al. (2020). Episignatures Stratifying Helsmoortel-Van Der Aa Syndrome Show Modest Correlation with Phenotype. Am J Hum Genet *107*, 555-563. 10.1016/j.ajhg.2020.07.003.
55. Cao, J., Spielmann, M., Qiu, X., Huang, X., Ibrahim, D.M., Hill, A.J., Zhang, F., Mundlos, S., Christiansen, L., Steemers, F.J., et al. (2019). The single-cell transcriptional landscape of mammalian organogenesis. Nature *566*, 496-502. 10.1038/s41586-019-0969-x.
56. Trapnell, C., Cacchiarelli, D., Grimsby, J., Pokharel, P., Li, S., Morse, M., Lennon, N.J., Livak, K.J., Mikkelsen, T.S., and Rinn, J.L. (2014). The dynamics and regulators of cell fate decisions are revealed by pseudotemporal ordering of single cells. Nat Biotechnol *32*, 381-386. 10.1038/nbt.2859.
57. Alcantara, S., Ruiz, M., D'Arcangelo, G., Ezan, F., de Lecea, L., Curran, T., Sotelo, C., and Soriano, E. (1998). Regional and cellular patterns of reelin mRNA expression in the forebrain of the developing and adult mouse. J Neurosci *18*, 7779-7799. 10.1523/JNEUROSCI.18-19-07779.1998.

58. Pesold, C., Impagnatiello, F., Pisu, M.G., Uzunov, D.P., Costa, E., Guidotti, A., and Caruncho, H.J. (1998). Reelin is preferentially expressed in neurons synthesizing gamma-aminobutyric acid in cortex and hippocampus of adult rats. Proc Natl Acad Sci U S A *95*, 3221-3226. 10.1073/pnas.95.6.3221.
59. Baran, Y., Bercovich, A., Sebe-Pedros, A., Lubling, Y., Giladi, A., Chomsky, E., Meir, Z., Hoichman, M., Lifshitz, A., and Tanay, A. (2019). MetaCell: analysis of single-cell RNA-seq data using K-nn graph partitions. Genome Biol *20*, 206. 10.1186/s13059-019-1812-2.
60. Cho, H., Yoo, T., Moon, H., Kang, H., Yang, Y., Kang, M., Yang, E., Lee, D., Hwang, D., Kim, H., et al. (2023). Adnp-mutant mice with cognitive inflexibility, CaMKIIalpha hyperactivity, and synaptic plasticity deficits. Mol Psychiatry *28*, 3548-3562. 10.1038/s41380-023-02129-5.
61. Delgado, R.N., Allen, D.E., Keefe, M.G., Mancia Leon, W.R., Ziffra, R.S., Crouch, E.E., Alvarez-Buylla, A., and Nowakowski, T.J. (2022). Individual human cortical progenitors can produce excitatory and inhibitory neurons. Nature *601*, 397-403. 10.1038/s41586-021-04230-7.
62. Ostapcuk, V., Mohn, F., Carl, S.H., Basters, A., Hess, D., Iesmantavicius, V., Lampersberger, L., Flemr, M., Pandey, A., Thoma, N.H., et al. (2018). Activity-dependent neuroprotective protein recruits HP1 and CHD4 to control lineage-specifying genes. Nature *557*, 739-743. 10.1038/s41586-018-0153-8.
63. Sun, X., Yu, W., Li, L., and Sun, Y. (2020). ADNP Controls Gene Expression Through Local Chromatin Architecture by Association With BRG1 and CHD4. Front Cell Dev Biol *8*, 553. 10.3389/fcell.2020.00553.
64. Clémot-Dupont, S., Lourenço Fernandes, J.A., Larrigan, S., Sun, X., Medisetti, S., Stanley, R., Hankouri, Z.E., Joshi, S.V., Picketts, D.J., Shekhar, K., and Mattar, P. (2024). The ChAHP chromatin remodelling complex regulates neurodevelopmental disorder risk genes to scale the production of neocortical layers. bioRxiv, 2024.2002.2012.579820. 10.1101/2024.02.12.579820.

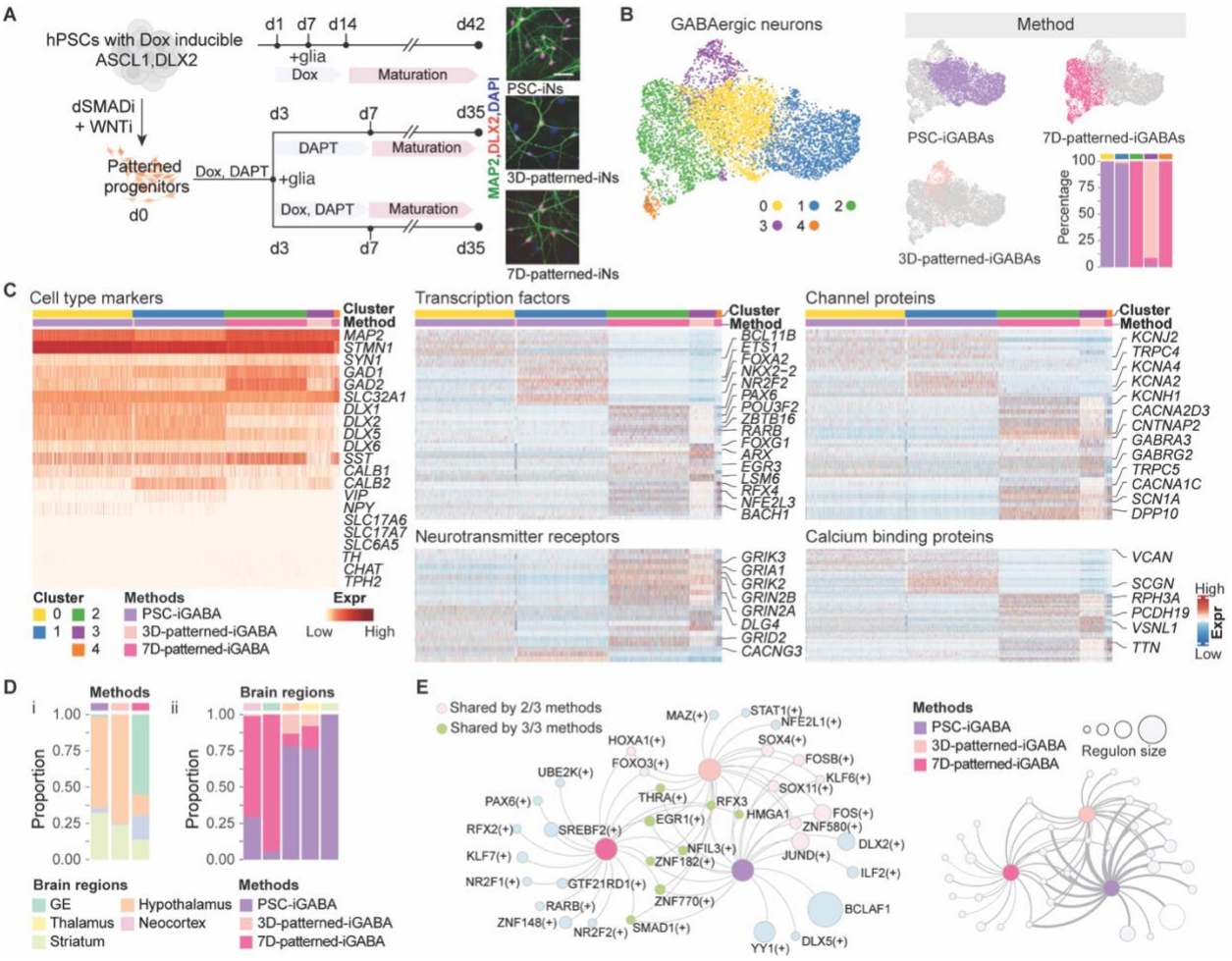

Figure 1. Generation of Diverse GABAergic iNs Using Different Strategies. (**A**) Schematic overview and timeline of the transcription factor (TF) and small molecule combinatory methods, followed by single-cell transcriptomics analysis. GABAergic neurons, marked by DLX2 and MAP2 expression, were generated using all three strategies. Scale bar, 50 µm. Abbreviations: dSMADi (dual SMAD inhibition), WNTi (WNT inhibition), PSC-iNs (PSC-derived induced neurons), 3DNPC-iNs (patterned induced neurons with 3 days of doxycycline exposure), and 7DNPC-iNs (patterned induced neurons with 7 days of doxycycline exposure). (**B**) UMAP embedding of *SCL32A1*-expressing GABAergic iNs, color-coded by cluster identity and differentiation method. The accompanying bar plot displays the percentage of cells from each method that belong to each cluster. (**C**) Heatmap analysis of cell type-specific markers, TFs, channel proteins, neurotransmitter receptors, and calcium-binding protein expression within each GABAergic iN cluster. The selected genes are implicated in psychiatric and neurological conditions, with a particular focus on ASD and epilepsy. (**D**) Percentage of cells from each method mapped to

distinct brain regions (left), alongside the contributions of each method to cells mapped to each brain region (right). (**E**) Gene Regulatory Network (GRN) analysis centered on method-specific modulators. Left: Each oval node represents a method linked to circular nodes representing associated regulons (TFs and their target genes). Regulons are color-coded based on uniqueness, with node size corresponding to the regulon size, indicating the number of target genes regulated by each TF. Right: The same GRN with edge thickness represents the strength of the association between method modulators and regulons. See also Figure S3, Table S2.

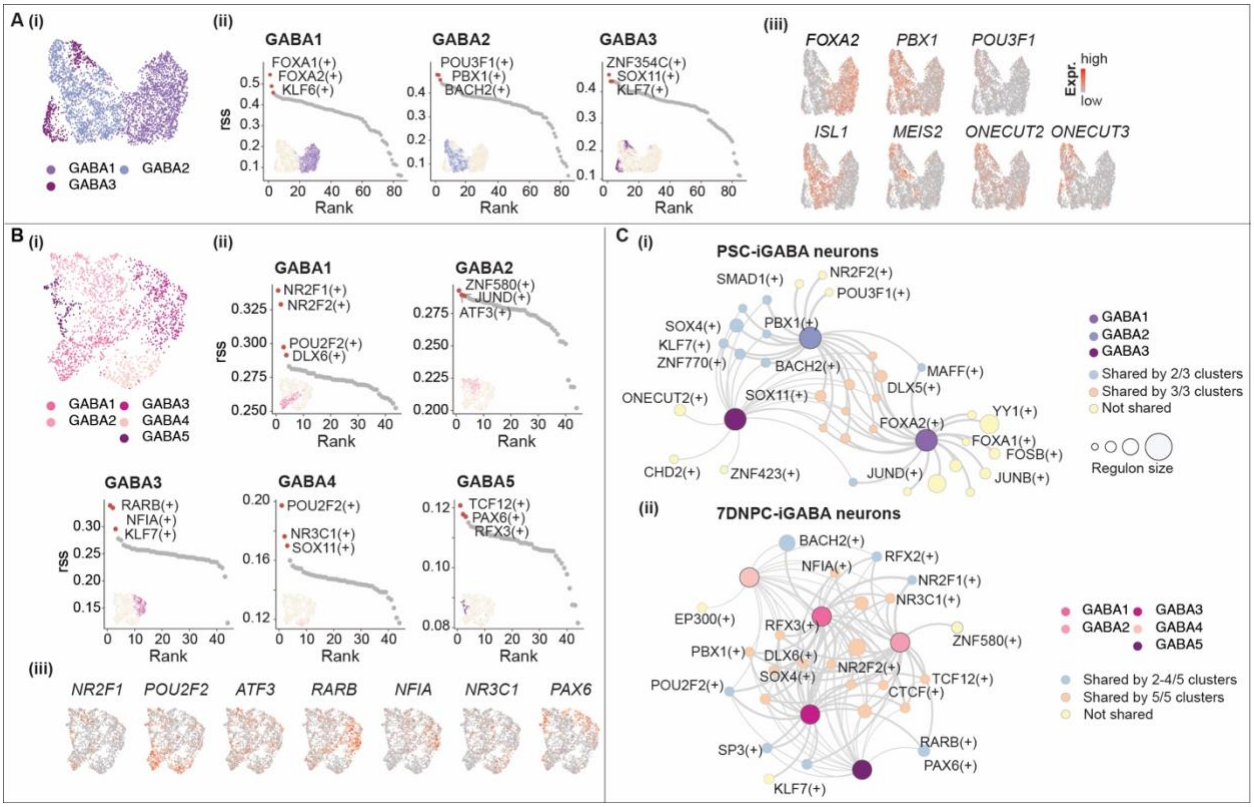

Figure 2. Gene Regulatory Networks Underlying Induced GABAergic Neuron Diversity. (A-B) Presented are the following for the GABAergic PSC-iNs (A) and the patterned iNs (B): (i) identified clusters, (ii) ranked regulons, and (iii) UMAP visualization of the top TFs associated with GABAergic neuron fate specification. **(C)** GRN analysis focused on cluster-specific modulators for **(i)** GABAergic PSC-iNs and **(ii)** patterned iNs. Each oval node represents a cluster connected to circular nodes that denote associated regulons. Regulons are color-coded based on uniqueness, with node size corresponding to the number of target genes regulated by each TF. Edge thickness indicates the strength of the association between cluster modulators and their corresponding regulons.

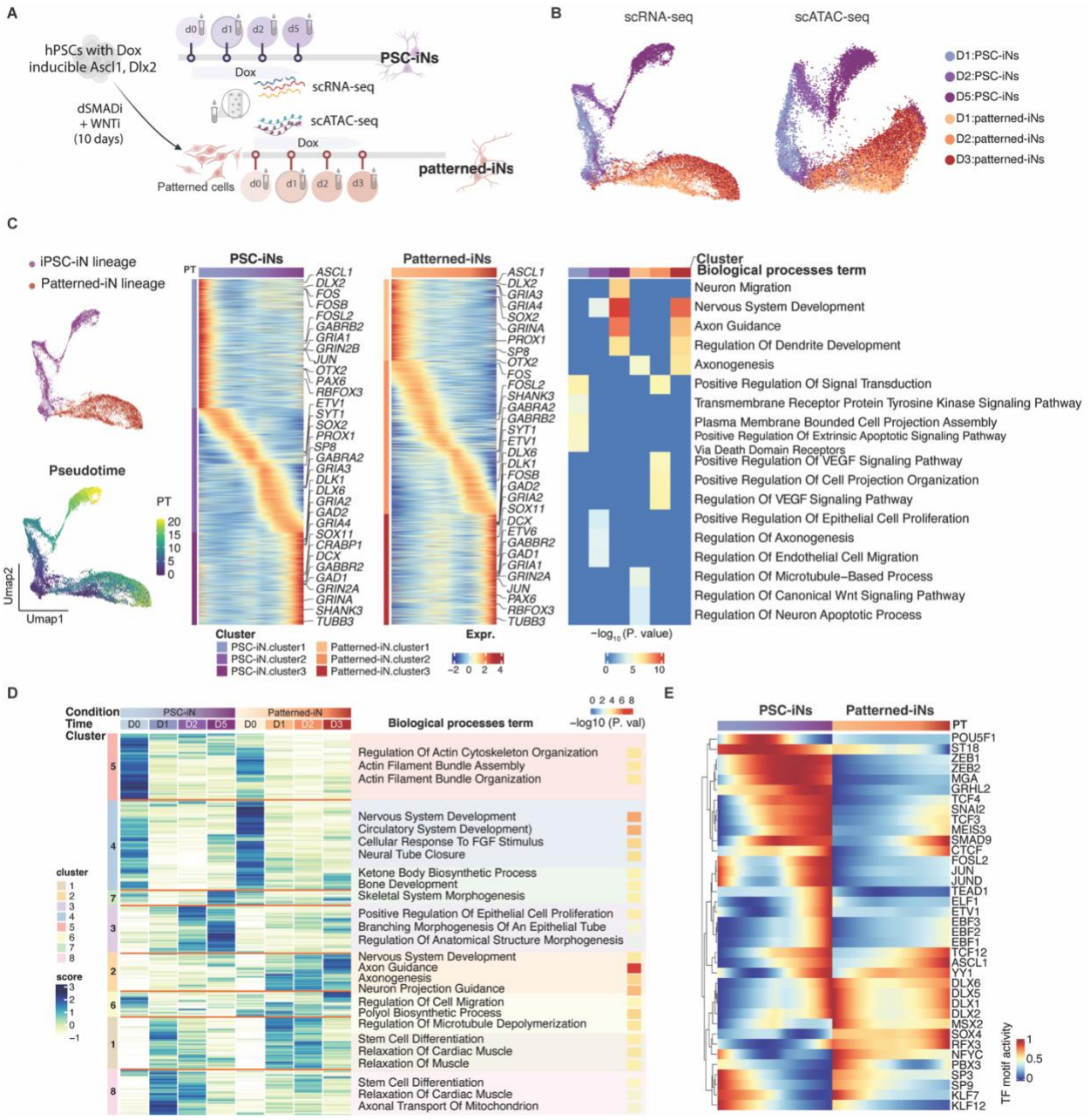

Figure 3. Molecular Signatures Underlying iN Specification. (A) Overview of the experimental workflow. **(B)** UMAP representations based on gene expression (left) and chromatin accessibility (right). Cells are color-coded according to differentiation time points and methods used. **(C)** UMAP of single-cell RNA sequencing (scRNA-seq) data highlighting the differentiation trajectory of PSC-iNs and patterned iNs, along with Slingshot-derived pseudotime (left). The middle panel shows a heatmap of gene expression across pseudotime bins within the PSC-iNs and patterned iNs trajectory. The right panel presents the Gene Ontology (GO) analysis of genes induced at various stages during early differentiation. **(D)** Heatmap showing the chromatin accessibility across

pseudobulk samples, aggregated from individual differentiation stages along the PSC-iNs and patterned iNs trajectory. The right panel shows the GO analysis of genes associated with accessible chromatin regions across the eight clusters. **(E)** Heatmaps showing motif activity of TFs across pseudotime bins. See also Figure S5.

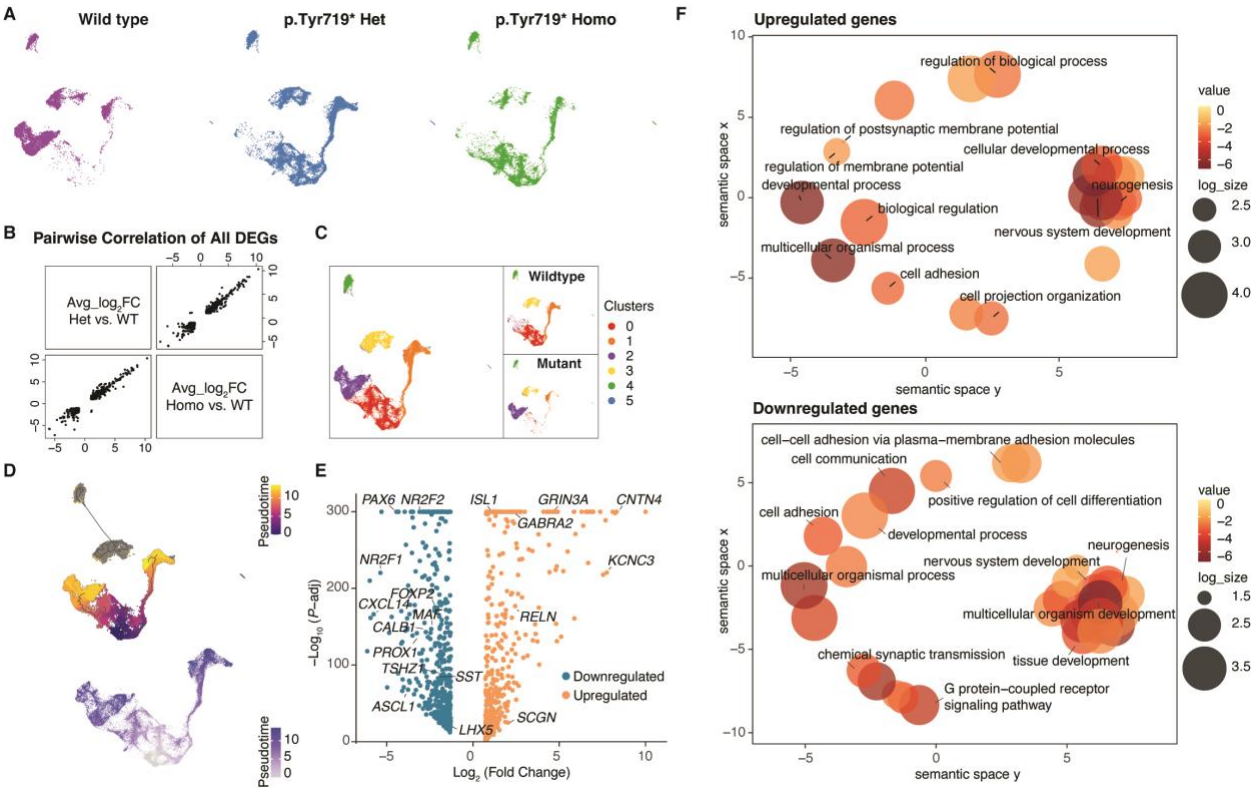

Figure 4. *ADNP* $^{p.Tyr719*}$ Mutation Disrupts Neurogenic and Synaptic Gene Expression. (A) Combined UMAP visualization of cells with the same genotype derived from different donor iPSCs. **(B)** Pairwise correlation analysis of all differentially expressed genes between mutant and wild-type cells, indicating similar transcriptional changes caused by both heterozygous and homozygous ADNPp.Tyr719* mutations. **(C)** Combined UMAP analysis of all cells, identifying clusters enriched in wild-type or mutant samples. Right panel: cells separated by genotype. **(D)** Pseudotime UMAP analysis of all cell types (top), and pseudotime value of clusters 0, 1, and 2 identified in (C) (bottom). **(E)** Volcano plot of DEGs (adjusted p-value < 0.05; |Log2(FC)| > 1) comparing ADNP$^{p.Tyr719*}$ samples to wild-type controls. Selected significantly downregulated and upregulated genes are labeled. **(F)** Top GO terms for Biological Processes associated with the genes depicted in (E). See also Figures S5, 6, 7 and Tables S4, 5, 6.

+STAR ★ Methods

Detailed methods are provided in the online version of this paper and include the following:

- **KEY RESOURCES TABLE**
- **RESOURCE AVAILABILITY**
  - Lead contact
  - Materials availability
  - Data and code availability
- **EXPERIMENTAL MODEL AND SUBJECT DETAILS**
  - Animal Model
  - iPSC lines and culture
  - Lentivirus production
  - Small molecule-mediated GABAergic neuron generation
  - TF-mediated induced GABAergic neuron generation
  - Patterned induced GABAergic neuron generation
  - Lentivirus production
  - Lentivirus transduction
- **METHOD DETAILS**
  - Primary mouse astrocytes
  - Immunofluorescence and imaging
  - Immunoblotting
  - 10X single-cell RNA-seq library preparation and sequencing
  - SHARE-seq library preparation and sequencing
- **QUANTIFICATION AND STATISTICAL ANALYSIS**
  - 10X Single-cell RNA-sequencing data processing and analysis
  - SHARE-seq data processing and analysis
  - Inferring regulatory networks
  - Gene Ontology and pathway enrichment analysis
  - WGCNA analysis
  - Statistical analyses

STAR ★ Methods

KEY RESOURCES TABLE

REAGENT or RESOURCE	SOURCE	IDENTIFIER
Antibodies		
Anti-ADNP	Bethyl Laboratories, Inc	Cat # A300-104A; RRID:AB_242522
Anti-HA	Roche	Cat #11867423001;RRID: AB_390918
Anti-CTCF	Cell Signaling Technology	Cat # 3418S; RRID:AB_2086791
Anti-HP1γ	Cell Signaling Technology	Cat # 2619S; RRID:AB_2070984
Anti-CHD4	Bethyl Laboratories, Inc	Cat # A301-081A; RRID:AB_873001
Anti-MAP2	Abcam	Cat # ab5392; RRID:AB_2138153
Anti-Synapsin	Synaptic Systems	Cat # 106 002; RRID:AB_887804
Anti-FOXG1	Takara Bio	Cat # M227; RRID:AB_2827749
Anti-Sox2	R&D Systems, Inc.	Cat # AF2018; RRID:AB_355110
Anti-Pax6	BioLegend	Cat # 901301; RRID:AB_2565003
Anti-H3K27ac	Abcam	Cat # AB4729; RRID:AB_2118291
Anti-IgG	Abcam	Cat # AB46540; RRID:AB_2614925
Anti-IgG	Novus Biologicals, LLC	Cat # NBP1-2763
Anti-FOS	Abcam	Cat # AB208942; RRID:AB_2747772
Anti-GAPDH	Cell Signaling Technology	Cat # 2118; RRID:AB_561053
Anti-β-actin	Sigma-Aldrich	Cat # A5441p RRID:AB_476744
Anti-Dlx5	(Wang et al., 2010)	Gift from John LR Rubenstein.
Anti-Dlx2	Santa Cruz Biotechnology, Inc	Cat # sc-393879
Peroxidase-AffiniPure Donkey Anti-Rabbit IgG	Jackson ImmunoResearch Labs	Cat# 711-035-152, RRID:AB_10015282
IRDye 680RD Donkey anti-Mouse IgG	LI-COR Biosciences	Cat# 926-68072, RRID:AB_10953628
IRDye 800CW Goat anti-Rat IgG	LI-COR Biosciences	Cat# 926-32219, RRID:AB_1850025
Donkey anti-Mouse IgG 488	Thermo Fisher Scientific	Cat# A-21202, RRID:AB_141607
Donkey anti-Mouse IgG 555	Thermo Fisher Scientific	Cat# A-31570, RRID:AB_2536180
Donkey anti-Rabbit IgG 555	Thermo Fisher Scientific	Cat# A-31572, RRID:AB_162543
Donkey anti-Rabbit IgG 488	Thermo Fisher Scientific	Cat# A-21206, RRID:AB_2535792
Donkey anti-Chicken IgG 647	Thermo Fisher Scientific	Cat# A78952, RRID:AB_2921074
Chemicals, peptides, and recombinant proteins		
Stemflex supplement	Gibco | Thermo Fisher Scientific	Cat # A33492

Stemflex basal media	Gibco | Thermo Fisher Scientific	Cat # A33493-01
MEM media	Gibco | Thermo Fisher Scientific	Cat # 11090-081
Neurobasal media	Gibco | Thermo Fisher Scientific	Cat # 21103-049
Naurobasal A media	Gibco | Thermo Fisher Scientific	Cat # 10888-022
DMEM/F12 media	Gibco | Thermo Fisher Scientific	Cat # 11320-033
DMEM media	Gibco | Thermo Fisher Scientific	Cat # 11965-092
Knockout DMEM	Gibco | Thermo Fisher Scientific	Cat # 10829018
B27 supplement	Gibco | Thermo Fisher Scientific	Cat # 17504-044
N2 supplement	Gibco | Thermo Fisher Scientific	Cat # 17502-048
KnockOut™ Serum Replacement	Gibco | Thermo Fisher Scientific	Cat # 10828028
MEM NEAA (100x)	Gibco | Thermo Fisher Scientific	Cat # 11140-050
Glutamax (100x)	Gibco | Thermo Fisher Scientific	Cat # 35050-061
Sodium Pyruvate (100x)	Gibco | Thermo Fisher Scientific	Cat # 11360-070
β-Mercaptoethanol	Sigma-Aldrich	Cat # M3148
Cosmic Calf™ Serum	Cytiva	Cat # SH3008704
Fetal Bovine Serum	Sigma-Aldrich	Cat # F6178
D-PBS tablets	Millipore	Cat # 524650-1EA
Geltrex	Gibco | Thermo Fisher Scientific	Cat # A14133-02
Poly-L-ornithine hydrobromide	Sigma-Aldrich	Cat # P3655
Accutase	Innovative Cell Technologies	Cat # AT104500
Trypsin 0.25%	Gibco | Thermo Fisher Scientific	Cat # 25200-114
Puromycin dihydrochloride	Sigma-Aldrich	Cat # P8833
Hygromycin B (50 mg/mL)	Gibco | Thermo Fisher Scientific	Cat # 10687010
Cytosine β-D-arabinofuranoside	Sigma-Aldrich	Cat # C1768
Doxycycline	Sigma-Aldrich	Cat # P3655
Bovine Serum Albumin	Equitech-Bio Inc	Cat # BAH65-0500
Thiazovivin	Santa Cruz Biotechnology, Inc	Cat # SC-361380
Y-27632	Tocris Bioscience	Cat # 1254
Chroman1	MedChemExpress LLC	Cat # HY-15392
LDN193189	Stemgent	Cat # 04-0074
SB431542	Tocris Bioscience	Cat # 1614
XAV939	Stemgent	Cat # 04-0046
DAPT	Tocris Bioscience	Cat # 2634
SHH	R&D Systems	Cat # 1845-SH
Purmorphamine	R&D Systems	Cat # SML0868

Dimethyl sulfoxide	Sigma-Aldrich	Cat # D2438
Paraformaldehyde solution	Affymetrix	Cat # 19943
Halt Protease and Phosphatase Inhibitor Cocktail	Thermo Fisher Scientific	Cat # 78440
Critical commercial assays		
Pierce RIPA Buffer	Thermo Fisher Scientific	Cat # 89900
Bolt™ 4 to 12%, Bis-Tris, Protein Gel	Thermo Fisher Scientific	Cat # MW04125BOX
iBlot™ 2 Transfer Stacks, PVDF	Thermo Fisher Scientific	Cat # IB24001
Western Lightning Plus, Chemiluminescent Substrate	Revvity Health Sciences Inc	Cat # NEL104001EA
Pierce™ BCA Protein Assay Kits	Thermo Fisher Scientific	Cat # 23225
Intercept® (PBS) Blocking Buffer	LI-COR bio	Cat # P/N: 927-70001
Bio Rad ChemiDoc MP Imaging System	Bio Rad	RRID:SCR_019037
Chromium Next GEM Single Cell 3' GEM Kit v3.1	10X Genomics	Cat # PN-1000123
Chromium Next GEM Single Cell 3' Gel Bead Kit v3.1	10X Genomics	Cat # PN-1000122
Chromium Next GEM Chip G Single Cell Kit	10X Genomics	Cat # PN-1000120
Chromium iX	10X Genomics	Cat # PN-1000328, RRID:SCR_024536
EVOS M5000 Imaging System	ThermoFisher Scientific	Cat # AMF5000, RRID:SCR_023650
Deposited Data		
Raw single cell-sequencing data and normalized counts	This paper	GSE277602 and GSE277604
Experimental models: cell lines		
PGP1	Coriell	Cat# GM23338, RRID:CVCL_F182
WTC11	Coriell	Cat# GM25256, RRID:CVCL_Y803
HES-3 NKX2.1GFP/w	Goulburn A.L., et al., 2011[1]	RRID:CVCL_A5HB
HEK293T	ATCC	Cat # 11268, RRID:CVCL_1926
Experimental models: organisms/strains		

CD1 mouse strain	Charles River	Cat# CRL:022, RRID:IMSR_CRL:022
Recombinant DNA		
FUW-M2rtTA	Hockemeyer et al., 2008[2]	RRID:Addgene_20342
TetO-Ascl1-puro	Yang et al., 2017[3]	RRID:Addgene_97329
TeoO-Dlx2-Hygro	Yang et al., 2017[3]	RRID:Addgene_97330
pMD2.G	Addgene	RRID:Addgene_12259
pRSV-rev	Addgene	RRID:Addgene_12253
pMDLg/pRRE	Addgene	RRID:Addgene_12251
PB-TO-ASCL1-DLX2	Addgene	RRID:Addgene_182307
Software and algorithms		
Cellranger v7.2.0	10x Genomics	RRID:SCR_023221
ClusterProfiler v4.8.3	Yu et al., 2012[4]	RRID:SCR_016884
DoubletFinder v2.0.4	McGinnis et al., 2019[5]	RRID:SCR_018771
Gephi v0.10.1	http://gephi.org/	RRID:SCR_004293
ggplot2 v3.4.3	Wickham, 2016[6]	RRID:SCR_014601
Metacell	Baran et a., 2019[7]	RRID:SCR_017013
Monocle3	Cao et al., 2019[8]	RRID:SCR_018685
R	Love et al., 2014[9]	https://www.r-project.org/
Revigo v1.8.1	Supek et al., 2011[10]	RRID:SCR_005825
RStudio v4.3.1	Rstudio team, 2020[11]	https://github.com/rstudio/
Seurat v4.0.1.	Butler et al., 2018[12]	RRID:SCR_016341
SingleCellExperiment v1.22.0	Amezquita et al., 2020[13]	https://github.com/drisso/SingleCellExperiment
Slingshot v2.8.0	Street et al., 2018[14]	RRID:SCR_017012

RESOURCE AVAILABILITY

Lead contact

Further information and requests for resources and reagents should be directed to and will be fulfilled by the Lead Contact, Nan Yang (nan.yang1@mssm.edu).

Materials availability

The plasmids and cell lines generated in this study will be made available on request upon the completion of a Material Transfer Agreement (MTA).

Data and code availability

Single-cell RNA-seq and SHARE-seq data have been deposited at GEO and are publicly available as of the date of publication. Accession numbers are listed in the key resources table.

The DOI is listed in the key resources table. This paper does not report original codes. Any additional information required to reanalyze the data reported in this paper is available from the lead contact upon request.

EXPERIMENTAL MODEL AND SUBJECT DETAILS

Animal Model

All animal experiments were approved by the Icahn School of Medicine at Mount Sinai Institutional Animal Care and Use Committee and were conducted in compliance with the relevant ethical regulations. Mice were maintained in social cages on a 12-hour light/dark cycle with free access to food and water; animals were monitored daily for food and water intake. Wild-type CD1 mice were used to isolate primary cell cultures on postnatal day 3 (P03). Animals of both sexes were used in the analyses.

iPSC lines and cell culture

Human PSCs were maintained on Geltrex-coated plates in Stemflex medium and a 5% CO2 environment at 37ºC. Cells were passaged using Accutase in Stemflex supplemented with Chroman1 (2 µM), which was removed from the media the following day.

To generate genetically modified PGP1 and WTC11 iPSCs with the *ADNP* p.Tyr719* variant, we altered the nucleotide sequence NM_015339.4.2157C to G. Additionally, we inserted hemagglutinin (HA) tags immediately after Tyr719 to detect the resulting truncated proteins. In parallel, as a control, we inserted HA tags at the 3' end of the endogenous ADNP gene in the PGP1 line. sgRNAs targeting proximal regions were designed using the CHOPCHOP online tool (https://chopchop.cbu.uib.no/) and cloned into the lentiCRISPRv1 plasmid (Addgene Plasmid #49535) using the Golden Gate Assembly protocol. The gene-targeting template plasmid used to generate the HA-tagged *ADNP* p.Tyr719* allele includes a puromycin-resistance cassette flanked by LoxP sites for Cre-recombinase mediated deletion, positioned after the HA tag sequence, and the 5′ and 3′ DNA homology arms. A similar gene-targeting template was used to generate the HA-tagged *ADNP* allele. The day before transfection, human iPSCs were dissociated into single cells with Accutase and plated at 250,000 cells per well in six-well plates containing StemFlex medium with Chroman1. For transfection, the template vector (1 µg) and the CRISPRv1-gRNA (0.5 µg) were incubated with Lipofectamine Stem Transfection Reagent (10 µl) and OptiMEM (250 µl, Invitrogen) for 10 minutes, then added dropwise to the iPSCs. Selection with puromycin (1µg/ml) in StemFlex medium started 24-48 hours after transfection and continued for approximately 10 days until stable colonies formed. Individual colonies were picked with a P200 pipette tip under a microscope. Heterozygous and homozygous ADNP p.Tyr719-HA* iPSC clones,

as well as heterozygous ADNP-HA iPSC clones, were confirmed by PCR. The puromycin-resistance cassette was removed using Cre-recombinase.

To generate iPSCs with stable inducible ASCL1-DLX2 integration, we took advantage of a bi-directional tetracycline-inducible promoter via the PiggyBac transposon system, as previously described [15]. The iPSCs were transfected with the PB-TO-ASCL1-DLX2 plasmid and the EF1a-transposase vector at a 2:1 ratio using Lipofectamine™ Stem Transfection Reagent. Selection with puromycin started 24-48 hours post-transfection and continued for 2 weeks. Successfully modified human iPSCs harboring stable TO-ASCL1-DLX2 integration were either cryopreserved for future applications or directly differentiated into neuronal cells. PB-TO-ASCL1-DLX2 (Addgene plasmid # 182307) and EF1a-transposase plasmid were gifts from iPSC Neurodegenerative Disease Initiative (iNDI) & Michael Ward.

Research on human-derived samples was conducted according to protocols approved by the institutional review boards of the Icahn School of Medicine at Mount Sinai.

Lentivirus production

Infectious lentiviral particles were produced in HEK293T cells using the third-generation lentiviral packaging plasmids: pMD2.G (Addgene plasmid # 12259), pRSV-rev (Addgene plasmid #: 12253), and pMDLg/pRRE (Addgene plasmid #: 12251) [16]. Lentiviruses were produced in HEK293T cells using polyethylenimine (PEI), following established protocols [17]. The lentiviral supernatant was centrifuged at 1,000g for 5 minutes to remove cellular debris. Lentiviral particles were then ultra-centrifuged, resuspended overnight with gentle shaking in DMEM, aliquoted, and stored at -80°C. Only virus preparations with >90% infection efficiency were used for experiments, as determined by GFP expression or antibiotic resistance.

Small molecule-mediated GABAergic neuron generation

Human PSCs were differentiated into cortical inhibitory neurons using an established protocol based on dual SMAD inhibition, WNT inhibition, and SHH activation,[18,19] with the following modifications. NKX2.1(GFP/w) cells were dissociated into single cells using Accutase and plated at 430,000 cells/cm² onto Geltrex-coated wells in KSR media (415 mL Knockout DMEM, 75 mL knockout serum replacement, 500 µL 2-mercaptoethanol, 5 mL NEAA, and 5 mL GlutaMAX) supplemented with 10 µM Y-27632. From days 1 to 10, the cells underwent daily complete medium changes with LDN193189 (100 nM), SB431542 (10 µM), and XAV939 (2 µM). During days 11 to 18, N2 medium supplemented with 1 µM Purmorphamine and 5 µM recombinant SHH was used to induce ventral identity. On day 32, NKX2.1-GFP cells were dissociated, collected via FACS, and replated with mouse glial cells. The cells were maintained in Neurobasal A media

supplemented with 1×B27, 1×Glutamax, 1% fetal bovine serum, and 2-4 μM AraC and harvested on day 67 for further analyses.

TF-mediated induced GABAergic neuron generation

We used our established protocol to generate GABAergic neurons through lentiviral-mediated overexpression of ASCL1 and DLX2, as previously described [3]. Briefly, PSCs were transduced with FUW-TetO-Ascl1-T2A-puromycin, FUW-TetO-Dlx2-IRES-hygromycin, and FUW-rtTA lentiviruses. Twenty-four hours later, the medium was replaced by N2 media (1×N2 supplement, 1×NEAA in DMEM-F12 media) supplemented with 2 μg/mL doxycycline to induce transgene expression. The transduced cells were selected for three days by applying hygromycin (200 μg/mL) and puromycin (1 μg/mL). Subsequently, the media was replaced with N2 media containing 4 μM AraC for an additional three days. On day 8, GABAergic neurons were co-cultured with mouse glial cells at a density of 104,000 cells/cm^2 on Geltrex-coated plates. Two weeks post-transgene induction, doxycycline was withdrawn, and the culture was maintained in Neurobasal A media supplemented with 1×B27, 1×Glutamax, and 1% fetal bovine serum. Mature neurons were used for various assays on day 35 after co-culture.

To generate GABAergic neurons from PSC lines with stable inducible ASCL1-DLX2 integration, PSCs were dissociated using Accutase and plated at a density of 100,000 cells/cm^2 on GelTrex -coated plates in StemFlex Medium supplemented with Chroman1. The following day, the medium was replaced with N2 media containing 2 μg/mL Doxycycline to induce the expression of ASCL1 and DLX2. After three days, 4 μM AraC was added to the N2 media. On day 8, the neurons were replated with mouse glial cells. All subsequent procedures followed the previously described protocol for generating GABAergic neurons using lentiviral vectors.

Patterned induced GABAergic neuron generation

PSC lines with stable inducible ASCL1-DLX2 integration were dissociated into single cells using Accutase and plated at 430,000 cells/cm² onto Geltrex-coated wells in KSR media supplemented with 2 μM Chroman1. From days 1 to 10, the cells underwent daily full medium changes with LDN193189 (100 nM), SB431542 (10 μM), and XAV939 (2 μM). Starting on day 11, N2 media supplemented with 2 μg/mL doxycycline and 10 μM DAPT (Tocris Bioscience, 2634) was used to induce ASCL1 and DLX2 expression and promote synchronized neural differentiation. Doxycycline was discontinued either 3 or 7 days later, and DAPT was removed after 7 days. Neurons were then dissociated and replated with mouse glial cells. Subsequent steps followed the established protocols used for other GABAergic neuron differentiation methods.

METHOD DETAILS

Primary mouse astrocytes

Mouse glial cultures were generated from cortical hemispheres at postnatal day 3 (P03). The cortices were incubated in 3 mL of 20 Units/mL Papain, 0.5 µM EDTA, and 1 µM CaCl2 in HBSS for 15 mins. After incubation, the tissues were manually dissociated by forceful trituration. The resulting cells were grown at 37°C with 5% CO_2 in DMEM media containing 1×NEAA, 1× sodium pyruvate, 10% Cytiva HyClone™ Cosmic Calf™ Serum (CCS), and 0.008% β-mercaptoethanol.

Immunofluorescence and imaging

Cultured cells were fixed with 4% paraformaldehyde in D-PBS at room temperature for 5-10 min. Cells were rinsed 3 times with D-PBS and subsequently permeabilized for 5 mins at room temperature with 0.2% Triton X-100 in D-PBS. After incubation in blocking buffer (4% bovine serum albumin (BSA) and 1% Cosmic Calf™ Serum in D-PBS) for 3 hours, primary antibodies were added for incubation overnight at 4˚C. After 3 rinses, cells were incubated with secondary antibodies in the blocking buffer for 3 h at room temperature. Images were acquired using the EVOS M5000 imaging system (Life Technologies).

Immunoblotting

Cells were washed three times with cold PBS, harvested using CELLTREAT cell lifters, and lysed with the RIPA Lysis and Extraction Buffer (supplemented with 1X Halt Protease and Phosphatase Inhibitor Cocktail and 5 mM EDTA). Cells were incubated on ice for 15 min with occasional vortexing, sonicated twice (1s pulse followed by 1 min on ice), incubated on ice for another 15 min with occasional vortexing, and then centrifuged at 21000 xg for 20 min with the supernatant collected for quantifications using the BCA assay. Samples were denatured with 1X NuPAGE LDS loading buffer (supplemented with 50 mM DTT) and incubated at 70 ºC for 10 min.

Approximately 25 µg of total proteins were loaded onto each well of the 4-12% Bis-Tris gel and run at 170 V for 30 min in 1X MOPS Buffer. Samples were then transferred onto PVDF membrane at 20 V for 1 h at 4 ºC in cold 1X Transfer Buffer (25 mM Tris, 200 mM Glycine, 15% MeOH in ddH2O), blocked with either the LICOR Blocking Buffer or 5% milk in TBST for 1h at RT, then incubated overnight at 4ºC on the rocking shaker with the addition of primary antibodies diluted in the corresponding blocking buffer supplemented with 0.1% Tween-20. Membranes were washed four times with TBST (5 min at RT on the shaker each time), incubated at RT for 1h with secondary antibodies (diluted in the corresponding blocking buffer and supplemented with 0.1% Tween-20 and 0.1% SDS), washed for another 4 times with TBST (for HRP antibodies, treated with the ECL buffer at A:B = 1:1 in dark for 5 min at RT before imaging), and imaged using the Bio-Rad ChemiDoc MP Imaging System.

10X single-cell RNA-seq library preparation and sequencing

We used a Papain solution to create single-cell suspensions based on a published method.[20] Neurons were detached from the plate using Accutase supplemented with 0.4% DNase (Worthington), collected and further dissociated with a Papain solution. This solution was prepared by adding 328 µL of Papain to each 20 mL Enzyme Stock Solution containing 1× EBSS, 0.46% D(+) Glucose, 26 mM NaHCO3, and 0.5 mM EDTA. Additionally, 0.004 g of L-cysteine was added before use. The solution was activated for 15 minutes at 37°C, followed by an additional 1.5-hour incubation at 37°C. Prepare the Inhibitor Stock Solution (0.46% D(+) Glucose and 25 mM NaHCO3 in1× EBSS), Low Ovo (10X) solution (3 g BSA (Sigma A8806), and 3 g Trypsin inhibitor (Worthington LS003086) in 200 mL D-PBS, adjusting the pH to 7.4) and High Ovo (5X) solution (6 g BSA and 6 g Trypsin inhibitor in 200 mL D-PBS, pH 7.4). The single-cell suspension was washed four times, alternating between low Ovo solution (9 mL inhibitor stock solution and 1 mL Low Ovo (10X)) and high Ovo solution (4 mL inhibitor stock solution and 1 mL High Ovo (5X)). After washing, the cells were centrifuged at 350 g for 5 minutes, and the resulting cell pellet was resuspended in cold 0.02% BSA. Single-cell RNA sequencing library preparation was performed using the Chromium Single Cell 3' Reagent V3 kit, following the manufacturer's specifications. Barcoded libraries were sequenced on the Illumina NovaSeq platform with 150 bp paired-end reads, achieving an average depth of approximately 30,000 reads per cell.

SHARE-seq library preparation and sequencing

SHARE-seq libraries were prepared as previously described[21]. Briefly, cells were fixed using 0.2% formaldehyde and permeabilized. For joint measurements of single-cell chromatin accessibility and expression (scATAC- and scRNA-seq), cells were first transposed by Tn5 transposase to mark regions of open chromatin. The mRNA was reverse transcribed using a poly(T) primer containing a unique molecular identifier (UMI) and a biotin tag. Permeabilized cells were distributed in a 96-well plate to hybridize well-specific barcoded oligonucleotides to transposed chromatin fragments and poly(T) cDNA. Hybridization was repeated three times to expand the barcoding space and ligate cell barcodes to cDNA and chromatin fragments. Reverse crosslinking was performed to release barcoded molecules. cDNA was separated from chromatin using streptavidin beads, and each library was prepared separately for sequencing. Libraries were sequenced on the Illumina NovaSeq platform (read 1: 50 cycles, read 2: 50 cycles, index 1: 99 cycles, index 2: 8 cycles).

QUANTIFICATION AND STATISTICAL ANALYSIS

10X Single-cell RNA-sequencing data processing and analysis

All single-cell RNA sequencing (scRNA-seq) samples were processed individually. Reads were aligned to the GRCh38 human and mm10 mouse reference transcriptomes (GRCh38_and_mm10-2020-A) using Cellranger (v7.0) with default parameters to generate count matrices. Subsequent analyses were performed in R using Seurat v5.0.1. The data was filtered to retain only genes annotated to the human genome, and features were retained if detected in at least 3 cells and with a minimum of 200 features per cell. High-quality cells were selected based on having 500 to 7,000 detected genes and a maximum of 20% of reads mapping to mitochondrial genes. For 7DNPC and ADNP neuron samples, doublets were removed using DoubletFinder (v2.0) with default parameters. After preprocessing, samples were merged and normalized using natural-log transformation, and counts were scaled by a factor of 10,000. Principal component analysis (PCA) was conducted on the 2,000 most variable features (FindVariableFeatures()). The first 20 principal components (k=20) were used to construct a K-nearest neighbor (KNN) graph, while the first 30 principal components were used for ADNP samples. Cells were clustered using the Louvain algorithm (FindClusters()) and visualized using UMAP embeddings. Clusters were manually annotated with cell types based on a curated list of markers (Table S2). When necessary, samples were integrated using the FastMNN algorithm (IntegrateLayers()). After merging or integration, genes related to the cell cycle and ribosomal function were regressed out. Differential expression analysis between clusters or samples was performed using the Wilcoxon rank sum test using only genes expressed by a minimum of 3-5% of cells. Method/cluster specificity genes were identified as previously described [22]. Briefly, genes with non-unique names or not expressed in any cells were filtered out. Gene expression was scaled to 1 million unique molecular identifiers per method or cluster. Gene expression specificity was calculated by dividing the expression of each gene in each method/cluster by the total expression of all genes in that method/cluster, resulting in values from 0 to 1, with values closer to 1 indicating high specificity. The top 10% of the most highly specific genes per method or cluster were used for gene expression analyses. Pseudotime trajectory analysis was performed using Slingshot (v2.7.0) or Monocle3 (v.1.3.7) software with default parameters. Graphtest() in Monocle3 was used to determine genes that change with pseudotime.

To assess the similarity of PSC-derived GABAergic neurons to inhibitory neurons from the developing fetal brain, we utilized previously published scRNA-seq data from Bhaduri et al. [23] encompassing weeks 18, 19, 20, and 25 of gestation across various brain regions (neocortex, striatum, thalamus, hypothalamus, ganglionic eminence, midbrain, and cerebellum). Additionally, hypothalamic neuron data from Herb et al. [24] were included. All datasets were merged into a single Seurat object for comprehensive analysis. The combined dataset was first refined to focus on

neurons expressing the inhibitory neuron makers GAD1/2 (log norm counts > 0). We employed Seurat's FindTransferAnchors() and MapQuery() functions for cell mapping and comparison. The data normalization was carried out using SCTransform.

SHARE-seq data processing and analysis

SHARE-seq libraries were aligned using a published pipeline (https://github.com/masai1116/SHARE-seq-alignmentV2). Briefly, SHARE-seq reads were trimmed and aligned to the hg38 genome using bowtie2. Reads were demultiplexed using four sets of 8-bp barcodes in the index reads, tolerating one mismatched base per barcode. Reads mapping to the mitochondria and chrY were discarded. Duplicates were removed based on the read alignment position and cell barcodes. Open chromatin region peaks were called on merged samples using MACS2. Peaks overlapping with ENCODE blacklisted regions (https://sites.google.com/site/anshulkundaje/projects/blacklists) were filtered out. Peak summits were extended by 250bp on each side and defined as accessible regions. The fragment counts in peaks and TF scores were calculated using chromVAR. SHARE-RNA-seq reads were aligned to the hg38 genome using STAR. Reads were demultiplexed as described above for SHARE-ATAC-seq. Aligned reads were annotated to both exons and introns using feature counts. PCR duplicates were removed based on UMIs and read alignment position. Cells that expressed >1,000 genes and <4% mitochondrial reads were retained. Seurat was used to preprocess the count matrix and cluster cells for scRNA-seq libraries as described above. For pseudotime trajectory analysis, hPSCs, NPC-like cells, and stressed cells were removed, and Slingshot was utilized with default parameters.

Inferring regulatory networks

To infer transcription factor (TF) regulon networks within our single-cell RNA-seq dataset, we utilized the SCENIC (Single-Cell rgulatory Network Inference and Clustering) [25] protocol (v1.1.2), which employs the vsn-pipeline version orchestrated via Nextflow with the pyscenic (v0.12.1) container. First, Seurat objects were converted into loom files using the SCopeLoomR package (v0.13.0). Subsequently, the pyscenic module was executed 20 times using its default settings. Only regulons identified in at least 15 out of the 20 runs were included for further analysis.

Gene Ontology and pathway enrichment analysis

We used Enrichr [26] to identify the cellular functions and biological processes of differentially expressed genes. To identify the cellular functions of differential peaks, we annotated the peaks to their nearest genes, followed by Enrichr analysis.

To determine the enrichment of genes implicated in autism spectrum disorder (ASD), we used the Simons Foundation Autism Research Initiative (SFARI) database to compile a list of 1,065 ASD-

associated genes scored 0-2 or categorized as syndromic. Fisher's exact test was performed to determine the statistical significance of the top 10% of differentially expressed genes specific to PSC-iGABAs or 7DNPC-iGABAs.

For a more comprehensive analysis of all neural-related diseases, we used the ToppGene Suite and selected the DisGeNET Curated database,[27] which includes a total of 11,181 annotations. DisGeNET integrates information on gene-disease associations from repositories, GWAS catalogs, animal models, and scientific literature. To control for multiple testing errors, a threshold of 0.05 was applied. We used a random sampling size of 5,000, considering only coding genes to ensure the results were not biased by the size of the gene list, and required a minimum feature count of at least two genes in our DEG list. Only disease associations with an FDR-adjusted p-value ≤ 0.05 (Benjamini-Hochberg for multiple hypothesis testing) were considered significant.

WGCNA analysis

A total of 8,516 genes with an average expression level above 0.15 were selected for WGCNA analysis.[28,29] To construct the network, a soft thresholding is selected through scale independence: power = 4 for clusters 0 and 2 and power = 3 for cluster 1. Gene clustering and module assignments were visualized using a dendrogram, highlighting the hierarchical relationships between gene modules.

Statistical analyses

Unless otherwise indicated, all data presented are the average of at least two biological replicates from each of at least two independent experiments. Statistical analysis was matched to the data structure as noted above in the Methods Details section for single-cell RNA-seq and SHARE-seq experiments. Statistical analyses were performed in RStudio (v4.3.1; RStudio team, 2020) or GraphPad Prism 9. See figure legends for details on specific statistical tests run for each experiment. Statistical significance is represented by a star (*) and indicates a computed P-value < 0.05. Graphs and plots were generated using Graphpad Prism or RStudio. Figures were generated using Adobe Illustrator and Biolegend.

1. Goulburn, A.L., Alden, D., Davis, R.P., Micallef, S.J., Ng, E.S., Yu, Q.C., Lim, S.M., Soh, C.L., Elliott, D.A., Hatzistavrou, T., et al. (2011). A targeted NKX2.1 human embryonic stem cell reporter line enables identification of human basal forebrain derivatives. Stem Cells *29*, 462-473. 10.1002/stem.587.
2. Hockemeyer, D., Soldner, F., Cook, E.G., Gao, Q., Mitalipova, M., and Jaenisch, R. (2008). A drug-inducible system for direct reprogramming of human somatic cells to pluripotency. Cell Stem Cell *3*, 346-353. 10.1016/j.stem.2008.08.014.
3. Yang, N., Chanda, S., Marro, S., Ng, Y.H., Janas, J.A., Haag, D., Ang, C.E., Tang, Y., Flores, Q., Mall, M., et al. (2017). Generation of pure GABAergic neurons by transcription factor programming. Nat Methods *14*, 621-628. 10.1038/nmeth.4291.

4. Wu, M., Shang, X., Sun, Y., Wu, J., and Liu, G. (2020). Integrated analysis of lymphocyte infiltration-associated lncRNA for ovarian cancer via TCGA, GTEx and GEO datasets. PeerJ *8*, e8961. 10.7717/peerj.8961.
5. McGinnis, C.S., Murrow, L.M., and Gartner, Z.J. (2019). DoubletFinder: Doublet Detection in Single-Cell RNA Sequencing Data Using Artificial Nearest Neighbors. Cell Syst *8*, 329-337 e324. 10.1016/j.cels.2019.03.003.
6. Wickham, H. (2016). ggplot2: Elegant Graphics for Data Analysis. Springer-Verlag New York.
7. Baran, Y., Bercovich, A., Sebe-Pedros, A., Lubling, Y., Giladi, A., Chomsky, E., Meir, Z., Hoichman, M., Lifshitz, A., and Tanay, A. (2019). MetaCell: analysis of single-cell RNA-seq data using K-nn graph partitions. Genome Biol *20*, 206. 10.1186/s13059-019-1812-2.
8. Cao, J., Spielmann, M., Qiu, X., Huang, X., Ibrahim, D.M., Hill, A.J., Zhang, F., Mundlos, S., Christiansen, L., Steemers, F.J., et al. (2019). The single-cell transcriptional landscape of mammalian organogenesis. Nature *566*, 496-502. 10.1038/s41586-019-0969-x.
9. Love, M.I., Huber, W., and Anders, S. (2014). Moderated estimation of fold change and dispersion for RNA-seq data with DESeq2. Genome Biol *15*, 550. 10.1186/s13059-014-0550-8.
10. Supek, F., Bosnjak, M., Skunca, N., and Smuc, T. (2011). REVIGO summarizes and visualizes long lists of gene ontology terms. PLoS One *6*, e21800. 10.1371/journal.pone.0021800.
11. team, R. (2020). RStudio: Integrated Development for R. RStudio. PBC, Boston, MA.
12. Butler, A., Hoffman, P., Smibert, P., Papalexi, E., and Satija, R. (2018). Integrating single-cell transcriptomic data across different conditions, technologies, and species. Nat Biotechnol *36*, 411-420. 10.1038/nbt.4096.
13. Amezquita, R.A., Lun, A.T.L., Becht, E., Carey, V.J., Carpp, L.N., Geistlinger, L., Marini, F., Rue-Albrecht, K., Risso, D., Soneson, C., et al. (2020). Orchestrating single-cell analysis with Bioconductor. Nat Methods *17*, 137-145. 10.1038/s41592-019-0654-x.
14. Street, K., Risso, D., Fletcher, R.B., Das, D., Ngai, J., Yosef, N., Purdom, E., and Dudoit, S. (2018). Slingshot: cell lineage and pseudotime inference for single-cell transcriptomics. BMC Genomics *19*, 477. 10.1186/s12864-018-4772-0.
15. Pantazis, C.B., Yang, A., Lara, E., McDonough, J.A., Blauwendraat, C., Peng, L., Oguro, H., Kanaujiya, J., Zou, J., Sebesta, D., et al. (2022). A reference human induced pluripotent stem cell line for large-scale collaborative studies. Cell Stem Cell *29*, 1685-1702 e1622. 10.1016/j.stem.2022.11.004.
16. Dull, T., Zufferey, R., Kelly, M., Mandel, R.J., Nguyen, M., Trono, D., and Naldini, L. (1998). A third-generation lentivirus vector with a conditional packaging system. J Virol *72*, 8463-8471. 10.1128/JVI.72.11.8463-8471.1998.
17. Longo, P.A., Kavran, J.M., Kim, M.S., and Leahy, D.J. (2013). Transient mammalian cell transfection with polyethylenimine (PEI). Methods Enzymol *529*, 227-240. 10.1016/B978-0-12-418687-3.00018-5.
18. Maroof, A.M., Keros, S., Tyson, J.A., Ying, S.W., Ganat, Y.M., Merkle, F.T., Liu, B., Goulburn, A., Stanley, E.G., Elefanty, A.G., et al. (2013). Directed differentiation and functional maturation of cortical interneurons from human embryonic stem cells. Cell Stem Cell *12*, 559-572. 10.1016/j.stem.2013.04.008.
19. Nicholas, C.R., Chen, J., Tang, Y., Southwell, D.G., Chalmers, N., Vogt, D., Arnold, C.M., Chen, Y.J., Stanley, E.G., Elefanty, A.G., et al. (2013). Functional maturation of hPSC-derived forebrain interneurons requires an extended timeline and mimics human neural development. Cell Stem Cell *12*, 573-586. 10.1016/j.stem.2013.04.005.

20. Zhang, Y., Sloan, S.A., Clarke, L.E., Caneda, C., Plaza, C.A., Blumenthal, P.D., Vogel, H., Steinberg, G.K., Edwards, M.S., Li, G., et al. (2016). Purification and Characterization of Progenitor and Mature Human Astrocytes Reveals Transcriptional and Functional Differences with Mouse. Neuron *89*, 37-53. 10.1016/j.neuron.2015.11.013.
21. Ma, S., Zhang, B., LaFave, L.M., Earl, A.S., Chiang, Z., Hu, Y., Ding, J., Brack, A., Kartha, V.K., Tay, T., et al. (2020). Chromatin Potential Identified by Shared Single-Cell Profiling of RNA and Chromatin. Cell *183*, 1103-1116 e1120. 10.1016/j.cell.2020.09.056.
22. Mullins, N., Forstner, A.J., O'Connell, K.S., Coombes, B., Coleman, J.R.I., Qiao, Z., Als, T.D., Bigdeli, T.B., Borte, S., Bryois, J., et al. (2021). Genome-wide association study of more than 40,000 bipolar disorder cases provides new insights into the underlying biology. Nat Genet *53*, 817-829. 10.1038/s41588-021-00857-4.
23. Bhaduri, A., Sandoval-Espinosa, C., Otero-Garcia, M., Oh, I., Yin, R., Eze, U.C., Nowakowski, T.J., and Kriegstein, A.R. (2021). An atlas of cortical arealization identifies dynamic molecular signatures. Nature *598*, 200-204. 10.1038/s41586-021-03910-8.
24. Herb, B.R., Glover, H.J., Bhaduri, A., Colantuoni, C., Bale, T.L., Siletti, K., Hodge, R., Lein, E., Kriegstein, A.R., Doege, C.A., and Ament, S.A. (2023). Single-cell genomics reveals region-specific developmental trajectories underlying neuronal diversity in the human hypothalamus. Sci Adv *9*, eadf6251. 10.1126/sciadv.adf6251.
25. Aibar, S., Gonzalez-Blas, C.B., Moerman, T., Huynh-Thu, V.A., Imrichova, H., Hulselmans, G., Rambow, F., Marine, J.C., Geurts, P., Aerts, J., et al. (2017). SCENIC: single-cell regulatory network inference and clustering. Nat Methods *14*, 1083-1086. 10.1038/nmeth.4463.
26. Chen, E.Y., Tan, C.M., Kou, Y., Duan, Q., Wang, Z., Meirelles, G.V., Clark, N.R., and Ma'ayan, A. (2013). Enrichr: interactive and collaborative HTML5 gene list enrichment analysis tool. BMC Bioinformatics *14*, 128. 10.1186/1471-2105-14-128.
27. Pinero, J., Ramirez-Anguita, J.M., Sauch-Pitarch, J., Ronzano, F., Centeno, E., Sanz, F., and Furlong, L.I. (2020). The DisGeNET knowledge platform for disease genomics: 2019 update. Nucleic Acids Res *48*, D845-D855. 10.1093/nar/gkz1021.
28. Langfelder, P., and Horvath, S. (2008). WGCNA: an R package for weighted correlation network analysis. BMC Bioinformatics *9*, 559. 10.1186/1471-2105-9-559.
29. Zhang, B., and Horvath, S. (2005). A general framework for weighted gene co-expression network analysis. Stat Appl Genet Mol Biol *4*, Article17. 10.2202/1544-6115.1128.